December 2012

Novel Methodology to Determine the Optimal Energy Storage Location in a Microgrid to Support Power Stability

Luis Fernando Montoya Sanchez
University of Wisconsin-Milwaukee

NOVEL METHODOLOGY TO DETERMINE THE OPTIMAL ENERGY STORAGE LOCATION IN A MICROGRID TO SUPPORT POWER STABILITY

by

Luis Fernando Montoya Sanchez

A Thesis Submitted in

Partial Fulfillment of the

Requirements for the Degree of

Master of Science

in Engineering

at

The University of Wisconsin-Milwaukee

December 2012

ABSTRACT

NOVEL METHODOLOGY TO DETERMINE THE OPTIMAL ENERGY STORAGE LOCATION IN A MICROGRID TO SUPPORT POWER STABILITY

by

Luis Fernando Montoya Sanchez

The University of Wisconsin-Milwaukee, 2012
Under the Supervision of David Yu, Ph.D

This thesis represents the result from a cooperation project, between the University of Wisconsin Milwaukee and Eaton corporation. Here, a new methodology to select the best location for storage in Microgrids is proposed, this methodology is an adaptation of a well known technique commonly used to solve the Power Flow in Power System planning analysis. This technique is known as the fully-coupled Newton Raphson methodology, and it commonly used to solve the power flow study analysis. Due to the large incorporation of renewable energy to distribution and subtransmission systems, the requirement of a method to quantify and select the optimal location for the energy storage system will allow Renewable Energy sources, to be integrated into Microgrids.

DEDICATED TO ABELARDO, NUBIA AND LAURA

"I love you my beautiful family" "Los amo mi hermosa familia"

Juan Marat: "There is no failure, except when we cease to strive"

TABLE OF CONTENTS

LIST OF FIGURES

LIST OF TABLES

ACKNOWLEDGMENTS

First I want to acknowledge and dedicate this thesis work to my family and god. My family has been fundamental in my life, and it is also because of their exceptional work, that I am the person I am.

Special thanks to my professor and advisor David Yu for believing in me, for giving me all this special and constant guidance and support during my Masters studies. Also, I want to thank him for all those great and long discussions, "thank you professor for instructing me in the art of Research".

Special thanks as well to Professor Adel Nasiri, for all his advices and guidance during the elaboration of this methodology, and for always bringing into the table those practical values that make our models more realistic. Also, special thanks to Dr. Vijay Bhavaraju from EATON Corp, thank you for all your innovative ideas, support, guidance and also for giving to my thesis that important industrial aspect.

Thank you to all my team members, and in special my peer, and good friend Qiang Fu. Thanks for all your support and extensive discussions. It has been a pleasure having you as part of my team.

Special thanks to my friend Zeljko for all those good discussions, and also for giving me amazing ideas in the development of this thesis work.

This material is based upon work supported by the Engineer Research and Development Center - Construction Engineering Research Laboratory (ERDCCERL) under Contract

No. W9132T-11-C-0022. Any opinions, findings and conclusions or recommendations expressed in this material are those of the author(s) and do not necessarily reflect the views of the ERDC-CERL.

1 Introduction

In the last decades Microgrids are receiving a lot of attention to provide higher energy surety, quality, and security while providing sustainability and energy efficiency.
A microgrid is defined as a network of loads and local generation (distributed generation), and also energy storage. Mainly, the presence of energy storage systems allows to regulate the voltage and frequency, while the system operates in different modes. For instance, when the microgrid is islanded from the utility grid. Therefore, due to the presence of high renewable energy penetration (intermittent) into the microgrid, maintaining the system at a stable operation is an outstanding issue.

1.1 Background

Most of the RENEWABLE SOURCE*s* and STORAGE DEVICEs are *connected to a microgrid through* INVERTERS*,* regardless of the nature or source of energy. This feature allows to establish and set up bidirectional controls for both, Active and Reactive power, or in other words, in both directions; *towards the grid and also towards the device.* Herein, the importance of having an energy storage element in a Microgrid is discussed in several papers[1]. The energy storage device should be able to apply voltage and frequency regulations throughout the Microgrid, that is why it is very important to quantify theoretically, the effectiveness of the energy storage device at a specific location inside of the Microgrid.

The methodology developed is based on the usage of the Jacobean matrices and determining the effect of active/reactive power variations at one node on magnitude and phase (voltage phasor), this is done if and only if, the power flow has converged, and the steady state Jacobean can be interpreted as a physical behavior. More detailed explanation of the calculations required will be shown in the next chapters.

2 Power Flow solution technique

As it is described on [2], the power flow (load flow) problem is at the heart of power system analysis.

The power flow solves the complex matrix equation:

$$YV = I = \frac{S^*}{V^*} \tag{2.1}$$

Where Y is the network nodal admittance matrix, V is the unknown complex node voltage vector, I is the nodal current injection vector, and $S = P + jQ$ is the apparent power nodal injection vector that represents the specified load and the generation at demand or generation nodes respectively.

In essence, the power flow equation is a non-linear equation, that has to be solved using a non-linear method to find the value of the unknowns. There are methods such as Gauss-Seidel, Newton-Raphson and Newton-Raphson decoupled, each one of the methods has certain advantages and disadvantages when solving the power flow.

In the power flow solution technique, a three phase bus can be classified according to the following table:

BUS TYPE	UNKNOWNS
PQ	The complex node voltage
PV	reactive power Q,and voltage phase δ
Slack Bus	Infinite source, active P and reactive Q are unknown

Table 1: Types of buses in the Power Flow problem

2.1 Newton-Raphson fully coupled method

This method is considered the most general and reliable method to solve the power flow equations. Once the equations for the power flow have been defined, the solution algorithm involves iteration based on successive linearizarion using the first term of a Taylor expansion of the equations to be solved.

First of all, the power flow equation using the power injected at node i, can be written as:

$$P_i - jQ_i = \sum_{k=1}^{n} \overline{Y}_{ik}\overline{V}_k\overline{V}_i^* \tag{2.2}$$

where,

$$\overline{Y}_{ik} = |\overline{Y}_{ik}|\angle\theta_{ik} \tag{2.3}$$

$$\overline{V}_k = |\overline{V}_k|\angle\delta_k \tag{2.4}$$

$$\overline{V}_i = |\overline{V}_i|\angle\delta_i \tag{2.5}$$

Thus, substituting equations (2.3)-(2.5) into equation (2.2) we get:

$$P_i - jQ_i = \sum_{k=1}^{n} |\overline{Y}_{ik}||\overline{V}_k||\overline{V}_i|\angle(\theta_{ik} - \delta_i + \delta_k) \tag{2.6}$$

Therefore, separating active and reactive power injections yields to:

$$P_i = \sum_{k=1}^{n} |\overline{Y}_{ik}||\overline{V}_k||\overline{V}_i|cos(\theta_{ik} - \delta_i + \delta_k) \tag{2.7}$$

$$Q_i = -\sum_{k=1}^{n} |\overline{Y}_{ik}||\overline{V}_k||\overline{V}_i|sin(\theta_{ik} - \delta_i + \delta_k) \tag{2.8}$$

Rearranging equation (2.7), the specified variable can be differentiated from the variable that is to be calculated, as shown in equation (2.9).

$$\{P_i\} - \left\{ \sum_{k=1}^{n} |\overline{Y}_{ik}||\overline{V}_k||\overline{V}_i| cos(\theta_{ik} - \delta_i + \delta_k) \right\} = 0 \tag{2.9}$$

$$\{Specified\, variable\} - \{variable\, to\, calculate\} = 0$$

There are some important observations from equation (2.7) and (2.8). In the case of classifying a node as the slack node, neither equation (2.7) nor (2.8) exist. If the type of node is a PQ node, both equations will exist. Also, if the node is a PV bus only equation (2.8) will exist in the solution of the method.

For n buses the Jacobean of the system will have the following form:

$$\begin{bmatrix} \triangle P_2 \\ \triangle P_3 \\ : \\ : \\ \triangle P_n \\ \triangle Q_2 \\ \triangle Q_3 \\ : \\ : \\ \triangle Q_n \end{bmatrix} = \begin{bmatrix} J_1 & J_2 \\ J_3 & J_4 \end{bmatrix} \begin{bmatrix} \triangle \delta_2 \\ \triangle \delta_3 \\ : \\ : \\ \triangle \delta_n \\ \triangle |V_2| \\ \triangle |V_3| \\ : \\ : \\ \triangle |V_n| \end{bmatrix} \tag{2.10}$$

In equation (2.10) four different groups are defined as:

$$J_1 = \begin{bmatrix} \frac{\partial P_2}{\partial \delta_2} & \frac{\partial P_2}{\partial \delta_3} & \cdots & \frac{\partial P_2}{\partial \delta_n} \\ \frac{\partial P_3}{\partial \delta_2} & \frac{\partial P_3}{\partial \delta_3} & \cdots & \frac{\partial P_3}{\partial \delta_n} \\ \vdots & \ddots & \cdots & \vdots \\ \frac{\partial P_n}{\partial \delta_2} & \frac{\partial P_n}{\partial \delta_3} & \cdot\cdot & \frac{\partial P_n}{\partial \delta_n} \end{bmatrix} \tag{2.11}$$

$$J_2 = \begin{bmatrix} \frac{\partial P_2}{\partial |V_2|} & \frac{\partial P_2}{\partial |V_3|} & \cdots & \frac{\partial P_2}{\partial |V_n|} \\ \frac{\partial P_2}{\partial |V_2|} & \frac{\partial P_2}{\partial |V_3|} & \cdots & \frac{\partial P_2}{\partial |V_n|} \\ \vdots & \ddots & \cdots & \vdots \\ \frac{\partial P_n}{\partial |V_2|} & \frac{\partial P_n}{\partial |V_3|} & \cdots & \frac{\partial P_n}{\partial |V_n|} \end{bmatrix} \tag{2.12}$$

$$J_3 = \begin{bmatrix} \frac{\partial Q_2}{\partial \delta_2} & \frac{\partial Q_2}{\partial \delta_3} & \cdots & \frac{\partial Q_2}{\partial \delta_n} \\ \frac{\partial P_3}{\partial \delta_2} & \frac{\partial P_3}{\partial \delta_3} & \cdots & \frac{\partial Q_3}{\partial \delta_n} \\ \vdots & \ddots & \cdots & \vdots \\ \frac{\partial Q_n}{\partial \delta_2} & \frac{\partial Q_n}{\partial \delta_3} & \cdot\cdot & \frac{\partial Q_n}{\partial \delta_n} \end{bmatrix} \tag{2.13}$$

$$J_4 = \begin{bmatrix} \frac{\partial Q_2}{\partial |V_2|} & \frac{\partial Q_2}{\partial |V_3|} & \cdots & \frac{\partial Q_2}{\partial |V_n|} \\ \frac{\partial Q_2}{\partial |V_2|} & \frac{\partial Q_2}{\partial |V_3|} & \cdots & \frac{\partial Q_2}{\partial |V_n|} \\ \vdots & \ddots & \cdots & \vdots \\ \frac{\partial Q_n}{\partial |V_2|} & \frac{\partial Q_n}{\partial |V_3|} & \cdots & \frac{\partial Q_n}{\partial |V_n|} \end{bmatrix} \tag{2.14}$$

Once equations (2.11) -(2.14) are plugged in equation (2.10) yields to:

$$\begin{bmatrix} \triangle P_2 \\ \triangle P_3 \\ \vdots \\ \vdots \\ \triangle P_n \\ \triangle Q_2 \\ \triangle Q_3 \\ \vdots \\ \vdots \\ \triangle Q_n \end{bmatrix} = \begin{bmatrix} \frac{\partial P_2}{\partial \delta_2} & \frac{\partial P_2}{\partial \delta_3} & \cdots & \frac{\partial P_2}{\partial \delta_n} & \frac{\partial P_2}{\partial |V_2|} & \frac{\partial P_2}{\partial |V_3|} & \cdots & \frac{\partial P_2}{\partial |V_n|} \\ \frac{\partial P_3}{\partial \delta_2} & \frac{\partial P_3}{\partial \delta_3} & \cdots & \frac{\partial P_3}{\partial \delta_n} & \frac{\partial P_2}{\partial |V_2|} & \frac{\partial P_2}{\partial |V_3|} & \cdots & \frac{\partial P_2}{\partial |V_n|} \\ \vdots & \ddots & \cdots & \vdots & \vdots & \ddots & \cdots & \vdots \\ \frac{\partial P_n}{\partial \delta_2} & \frac{\partial P_n}{\partial \delta_3} & .. & \frac{\partial P_n}{\partial \delta_n} & \frac{\partial P_n}{\partial |V_2|} & \frac{\partial P_n}{\partial |V_3|} & \cdots & \frac{\partial P_n}{\partial |V_n|} \\ \frac{\partial Q_2}{\partial \delta_2} & \frac{\partial Q_2}{\partial \delta_3} & \cdots & \frac{\partial Q_2}{\partial \delta_n} & \frac{\partial Q_2}{\partial |V_2|} & \frac{\partial Q_2}{\partial |V_3|} & \cdots & \frac{\partial Q_2}{\partial |V_n|} \\ \frac{\partial P_3}{\partial \delta_2} & \frac{\partial P_3}{\partial \delta_3} & \cdots & \frac{\partial Q_3}{\partial \delta_n} & \frac{\partial Q_2}{\partial |V_2|} & \frac{\partial Q_2}{\partial |V_3|} & \cdots & \frac{\partial Q_2}{\partial |V_n|} \\ \vdots & \ddots & \cdots & \vdots & \vdots & \ddots & \cdots & \vdots \\ \frac{\partial Q_n}{\partial \delta_2} & \frac{\partial Q_n}{\partial \delta_3} & .. & \frac{\partial Q_n}{\partial \delta_n} & \frac{\partial Q_n}{\partial |V_2|} & \frac{\partial Q_n}{\partial |V_3|} & \cdots & \frac{\partial Q_n}{\partial |V_n|} \end{bmatrix} \begin{bmatrix} \triangle \delta_2 \\ \triangle \delta_3 \\ \vdots \\ \vdots \\ \triangle \delta_n \\ \triangle |V_2| \\ \triangle |V_3| \\ \vdots \\ \vdots \\ \triangle |V_n| \end{bmatrix} \tag{2.15}$$

Equation (2.15) represents the Jacobean Matrix of the system. Here, the Taylor expansion previously mentioned is considered, but just the first partial derivatives are considered, as it is enlightened in [2]. It is essential to mention that in principle the Jacobean matrix is not giving a physical sense of the system behavior, but once the iteration process has converged different convergence points that will appear (different operating points, or loading) can be analyzed. The topic about the non convergence of the power flow will be mentioned further in a chapter dedicated to power stability.

3 Stability Analysis based on the Power Flow Solution

This chapter has been created to specify the advantages of the power flow solution in the analysis of stability in the system. First, let us start saying that if the Newton-Raphson method is used to solve the power flow, the aforementioned four derivatives have to be calculated. But once the power flow has converged, a concept known as the modal Analysis can be done.

In essence, an equation that will look like equation (3.1) can be obtained.

$$\begin{bmatrix} \triangle P \\ \triangle Q \end{bmatrix} = \begin{bmatrix} J_{P\theta} & J_{PV} \\ J_{Q\theta} & J_{QV} \end{bmatrix} \begin{bmatrix} \triangle \theta \\ \triangle V \end{bmatrix} \tag{3.1}$$

If the eigenvalues of the Jacobean matrix are computed, the principal directions of change of the linearized version of the system can be observed. Therefore, if the eigenvalues are calculated for a set of different operating points or load flows, a trend of how the system operates can be visualized.

A concept that has to be discussed at this point, is the one related to the concept of stable or unstable solution. It is expected that an injection of active power at some distributed location, will produce a decrease in the voltage phasor phase angle; if the reference is defined as the slack bus phase. So on, an increase in the active power demanded at some location will produce an increase of the voltage phasor angle, due to the fact that extra power has to be exported through the lines of the system. The same idea applies for reactive power demand increase or decrease (generation) and the variation of the voltage phasor magnitude.

A very important and clue concept that comes precisely in this analysis, is the coupling between active power and phase angle, and also a coupling between reactive power and voltage phasor magnitude. But, this concept is only true when the analysis is being done at transmission level, since the inductive reactance of the line is at least ten or twenty times

much greater than the line resistance.

Two other ways to decouple the active and reactive power are also defined in the literature [2]. If the steady state has been reached, the $\triangle P$ can be considered to be close to zero. As a result, equation (3.1) can be split in two different equations:

$$\triangle P = 0 = J_{P\theta} \triangle \theta + J_{PV} \triangle V \tag{3.2}$$

$$\triangle Q = J_{Q\theta} \triangle \theta + J_{QV} \triangle V \tag{3.3}$$

Therefore, equation (3.2) can be simplified as shown in equation (3.4), if it is solved for $\triangle \theta$ it yields to:

$$\triangle \theta = J_{P\theta}^{-1} J_{PV} \triangle V \tag{3.4}$$

Then, if equation (3.4) is substituted into equation (3.3) the following relation can be obtained:

$$\triangle Q = (J_{Q\theta} J_{P\theta}^{-1} J_{PV} + J_{QV}) \triangle V \tag{3.5}$$

In this way, a new Jacobean sub-matrix can be formed. So on, the eigenvalues for a particular load flow condition and line impedance infrastructure, can be analyzed at some steady state operating condition to determine whether or not, the system is operating at a stable condition. According to reference [1], all the eigenvalues should be positive or in other words, they should be located on the right side of the complex plane.

This means that any reactive power injection will result in a voltage phasor magnitude increase. Also, it can has to be mentioned that another Jacobean sub-matrix can be calculated, but considering the relationship between eigenvalues can be calculated in the

original Jacobean, in which none consideration is required in terms of considering $\triangle P = 0$ or $\triangle Q = 0$. Also, the idea of considering that all the eigenvalues should be on the left side of the complex plane holds for this case, so in this sense, the solution is considered stable if all the eigenvalues appear on the right side of the complex plane. It should be mentioned, that when the calculation of the eigenvalues is done directly without considering any special assumption, it is possible to obtain so complex eigenvalues as well.

4 Adaptation & Formulation of the sensitivity analysis

In order to describe a framework of how the Newton-Raphson methodology could be adapted to select the best location for the storage, it is necessary to refer to equation (2.15). First, let us say, once the steady state has been accomplished, after solving the power flow non-linear equations. The inverse of the Jacobean Matrix can be calculated at the steady state solution, and the terms involved in the matrix inverse will have a structure as the one shown in equation (4.1).

$$\begin{bmatrix} \frac{\partial \delta_2}{\partial P_2} & \frac{\partial \delta_2}{\partial P_3} & \cdots & \frac{\partial \delta_2}{\partial P_n} & \frac{\partial \delta_2}{\partial Q_2} & \frac{\partial \delta_2}{\partial Q_3} & \cdots & \frac{\partial \delta_2}{\partial Q_n} \\ \frac{\partial \delta_3}{\partial P_2} & \frac{\partial \delta_3}{\partial P_3} & \cdots & \frac{\partial \delta_3}{\partial P_n} & \frac{\partial \delta_3}{\partial Q_2} & \frac{\partial \delta_3}{\partial Q_3} & \cdots & \frac{\partial \delta_3}{\partial Q_n} \\ \vdots & \vdots & \cdots & \vdots & \vdots & \vdots & \cdots & \vdots \\ \frac{\partial \delta_n}{\partial P_2} & \frac{\partial \delta_n}{\partial P_3} & \cdots & \frac{\partial \delta_n}{\partial P_n} & \frac{\partial \delta_n}{\partial Q_2} & \frac{\partial \delta_n}{\partial Q_3} & \cdots & \frac{\partial \delta_n}{\partial Q_n} \\ \frac{\partial |V_2|}{\partial P_2} & \frac{\partial |V_2|}{\partial P_3} & \cdots & \frac{\partial |V_2|}{\partial P_n} & \frac{\partial |V_2|}{\partial Q_2} & \frac{\partial |V_2|}{\partial Q_3} & \cdots & \frac{\partial |V_2|}{\partial Q_n} \\ \frac{\partial |V_3|}{\partial P_2} & \frac{\partial |V_3|}{\partial P_3} & \cdots & \frac{\partial |V_3|}{\partial P_n} & \frac{\partial |V_3|}{\partial Q_2} & \frac{\partial |V_3|}{\partial Q_3} & \cdots & \frac{\partial |V_3|}{\partial Q_n} \\ \vdots & \vdots & \cdots & \vdots & \vdots & \vdots & \cdots & \vdots \\ \frac{\partial |V_n|}{\partial P_2} & \frac{\partial |V_n|}{\partial P_3} & \cdots & \frac{\partial |V_n|}{\partial P_n} & \frac{\partial |V_n|}{\partial Q_2} & \frac{\partial |V_n|}{\partial Q_3} & \cdots & \frac{\partial |V_n|}{\partial Q_n} \end{bmatrix} \begin{bmatrix} \triangle P_2 \\ \triangle P_3 \\ \vdots \\ \triangle P_n \\ \triangle Q_2 \\ \triangle Q_3 \\ \vdots \\ \triangle Q_n \end{bmatrix} = \begin{bmatrix} \triangle \delta_2 \\ \triangle \delta_3 \\ \vdots \\ \triangle \delta_n \\ \triangle |V_2| \\ \triangle |V_3| \\ \vdots \\ \triangle |V_n| \end{bmatrix} \tag{4.1}$$

4.1 Steady state solution interpretation

In this chapter, the main purpose is to discuss the idea of using the Jacobean inverse as an accurate way to define a weighted measurement to select the best location for the storage. Let us say, there is a simplified Microgrid as the one shown in Figure (4.1), in this case there are n possible locations for the storage that can be analyzed through the power flow methodology once it converges. As it was mentioned before, all four derivatives will appear only if the node is defined as a PQ node; either injecting or consuming active or reactive

power (feature that is available since there is an inverter as the interface between the device and the grid connecting point). Therefore, all nodes are defined as PQ buses except for the slack bus, and in this way all four derivatives can be obtained for n locations in the system (the slack bus is excluded and has to be defined).

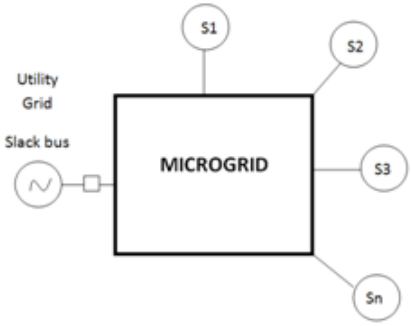

Figure 4.1: Microgrid structure in the case of n possible locations.

Previously in this chapter, a description of the Jacobean inverse was shown. Herein, as shown in equation (4.1), it is important to highlight the fact that the columns of the inverse matrix are derivatives of both δ(voltage phasor phase angle) and $|V|$(voltage phasor magnitude) for all the PQ nodes, with respect to an active/reactive power change at a particular place. In other words, the columns of the Jacobean inverse will define four different groups of derivatives, that basically will describe the impact in all different locations, due to a change in active/reactive power at some particular location. These four different types of derivatives obtained at the steady state are shown in equation (4.2). This methodology has an immediate predecessor, that is the methodology used for QV analysis, also called reactive power support. In this original methodology a subjacobian matrix is inverted, as the one shown in equation (3.5). Herein, and based on the values obtained for $\frac{\partial Q}{\partial V}$, designers have selected places in Power System configurations, where the effect of installing capacitor banks has a high impact in the voltage stability. A clear example of this methodology can be found in [2].

$$\begin{bmatrix} \frac{\partial \delta_2}{\partial P_2} & \frac{\partial \delta_2}{\partial P_3} & \cdots & \frac{\partial \delta_2}{\partial P_n} & \frac{\partial \delta_2}{\partial Q_2} & \frac{\partial \delta_2}{\partial Q_3} & \cdots & \frac{\partial \delta_2}{\partial Q_n} \\ \frac{\partial \delta_3}{\partial P_2} & \frac{\partial \delta_3}{\partial P_3} & \cdots & \frac{\partial \delta_3}{\partial P_n} & \frac{\partial \delta_3}{\partial Q_2} & \frac{\partial \delta_3}{\partial Q_3} & \cdots & \frac{\partial \delta_3}{\partial Q_n} \\ \vdots & \vdots & \cdots & \vdots & \vdots & \vdots & \cdots & \vdots \\ \frac{\partial \delta_n}{\partial P_2} & \frac{\partial \delta_n}{\partial P_3} & \cdots & \frac{\partial \delta_n}{\partial P_n} & \frac{\partial \delta_n}{\partial Q_2} & \frac{\partial \delta_n}{\partial Q_3} & \cdots & \frac{\partial \delta_n}{\partial Q_n} \\ \frac{\partial |V_2|}{\partial P_2} & \frac{\partial |V_2|}{\partial P_3} & \cdots & \frac{\partial |V_2|}{\partial P_n} & \frac{\partial |V_2|}{\partial Q_2} & \frac{\partial |V_2|}{\partial Q_3} & \cdots & \frac{\partial |V_2|}{\partial Q_n} \\ \frac{\partial |V_3|}{\partial P_2} & \frac{\partial |V_3|}{\partial P_3} & \cdots & \frac{\partial |V_3|}{\partial P_n} & \frac{\partial |V_3|}{\partial Q_2} & \frac{\partial |V_3|}{\partial Q_3} & \cdots & \frac{\partial |V_3|}{\partial Q_n} \\ \vdots & \vdots & \cdots & \vdots & \vdots & \vdots & \cdots & \vdots \\ \frac{\partial |V_n|}{\partial P_2} & \frac{\partial |V_n|}{\partial P_3} & \cdots & \frac{\partial |V_n|}{\partial P_n} & \frac{\partial |V_n|}{\partial Q_2} & \frac{\partial |V_n|}{\partial Q_3} & \cdots & \frac{\partial |V_n|}{\partial Q_n} \end{bmatrix} \begin{bmatrix} \triangle P_2 \\ \triangle P_3 \\ \vdots \\ \triangle P_n \\ \triangle Q_2 \\ \triangle Q_3 \\ \vdots \\ \triangle Q_n \end{bmatrix} = \begin{bmatrix} \triangle \delta_2 \\ \triangle \delta_3 \\ \vdots \\ \triangle \delta_n \\ \triangle |V_2| \\ \triangle |V_3| \\ \vdots \\ \triangle |V_n| \end{bmatrix} \tag{4.2}$$

4.2 Jacobean inverse & Indexes proposed

Initially it is necessary to go back to the idea of steady state solution (where generation and load meet each other). Once this condition is accomplished, based on equation (4.2) four indexes are described per node i as:

$$Index_{1i} = \frac{\sum_{k=1}^{n} \frac{\partial \delta_k}{\partial P_i}}{n} \tag{4.3}$$

$$Index_{2i} = \frac{\sum_{k=1}^{n} \frac{\partial |V|_k}{\partial P_i}}{n} \tag{4.4}$$

$$Index_{3i} = \frac{\sum_{k=1}^{n} \frac{\partial \delta_k}{\partial Q_i}}{n} \tag{4.5}$$

$$Index_{4i} = \frac{\sum_{k=1}^{n} \frac{\partial |V|_k}{\partial Q_i}}{n} \tag{4.6}$$

The indexes are the summation of the columns of the Inverted Jacobean matrix divided

by the number of nodes, and also define a mathematical weighted measurement to define if a location is more suitable for the storage placement. Therefore, active/reactive power injection or absorption would be more effective to back up voltage, and frequency.

In the power system, and specifically in Microgrids the roll of storage is to maintain the system voltages and frequency (phase) in normal conditions. Reference [5]is the Power Quality standard that is approved by the IEEE Smart Grid Standard. This standard proposes voltage should be in the range of 1.05 and 0.9 $p.u.$, and frequency in the range of $\pm 5\%$, which is the main objective in the operation of the Battery Storage for Microgrids.

4.3 Steady state example of the methodology Application

In order to show an interactive example of this methodology, the 14 Bus IEEE Transmission System was chosen. Information regarding this system can be found in [9]. This system is shown in figure (4.2), and as it was aforementioned all buses are modeled as PQ buses except for the slack bus which is bus one.

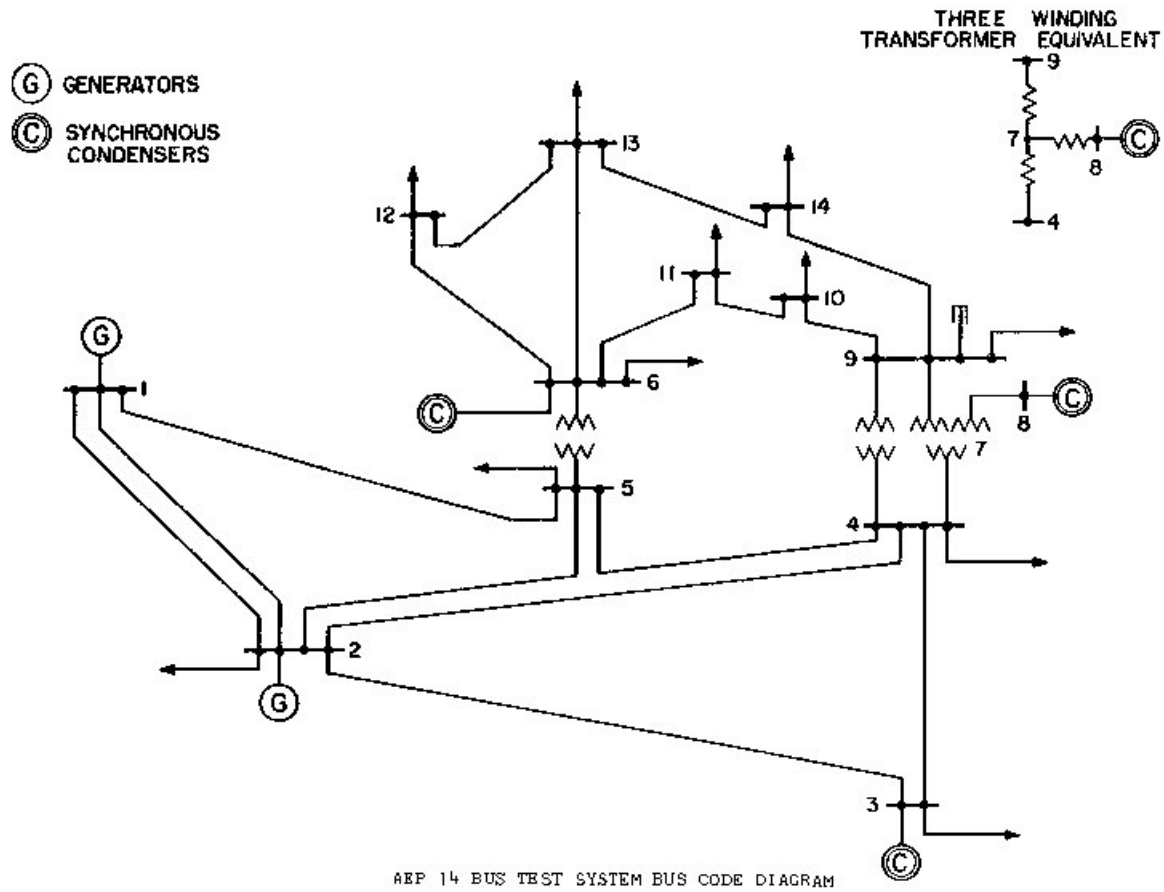

Figure 4.2: 14 Bus Transmission System IEEE. `http://sys.elec.kitami-it.ac.jp/ueda/demo/PFdata/`

The system running at the rated load, has a total power generation of 278MW and 111.67MVAr coming from the slack bus, and 259MW - 73.5MVAr load. In addition, this system has 19.238 MW of active power losses in the lines.

Once an initial framework for the normal operation of the system has been mentioned, a small active power change is forced at bus 3 of the system. The interval of active power change forced at bus 3 goes from generating 200MW at node 3, to an increase in the demand of a 100MW. This increase and decrease in active power is done around the rated load value of this bus. Therefore, the four indexes proposed are calculated, and the results are shown in Figure (4.3)-(4.6).

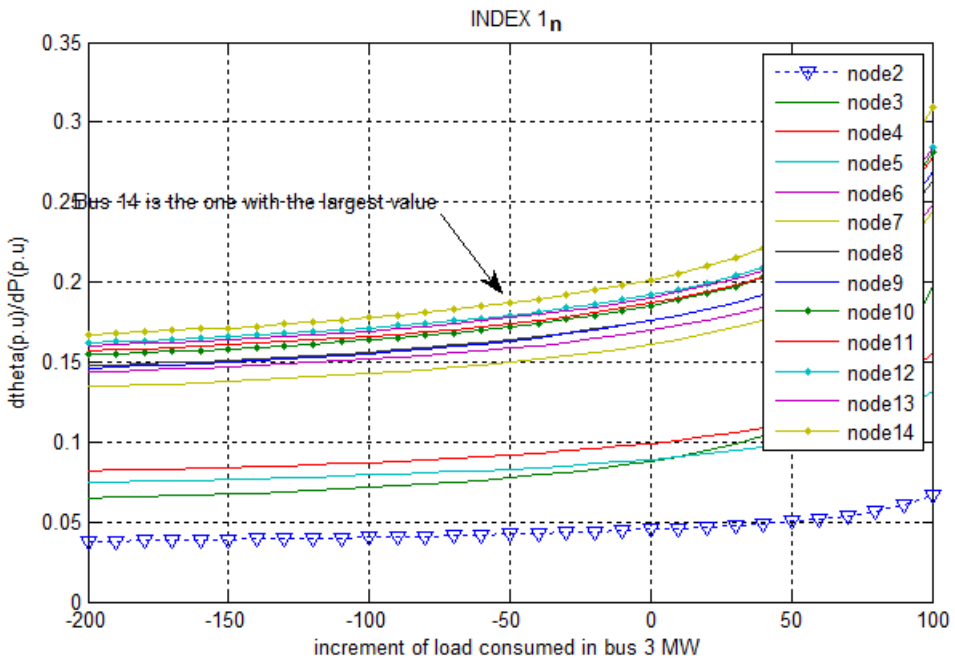

Figure 4.3: Index I obtained when changing the load at bus 3

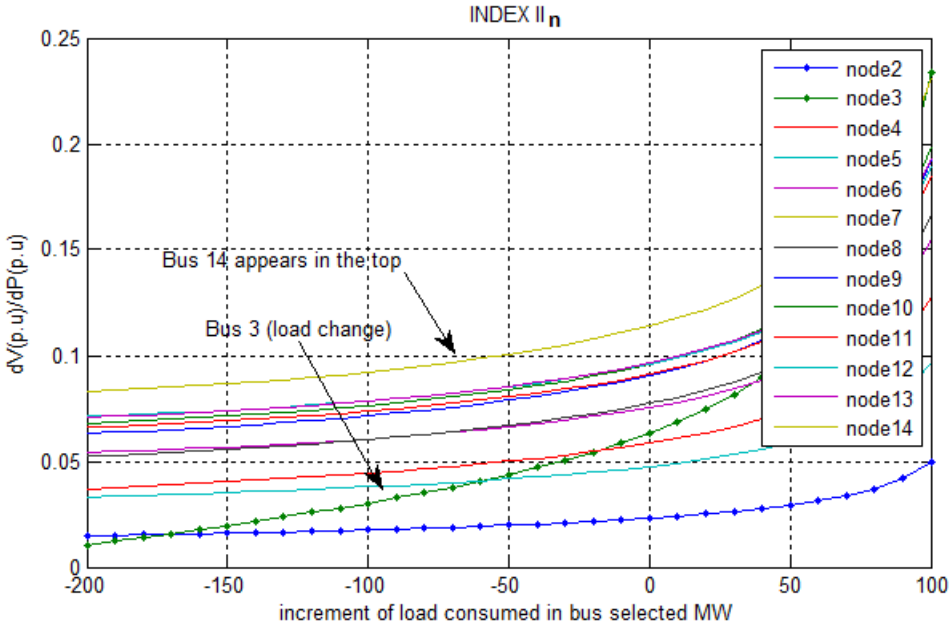

Figure 4.4: Index II obtained when changing the load at bus 3

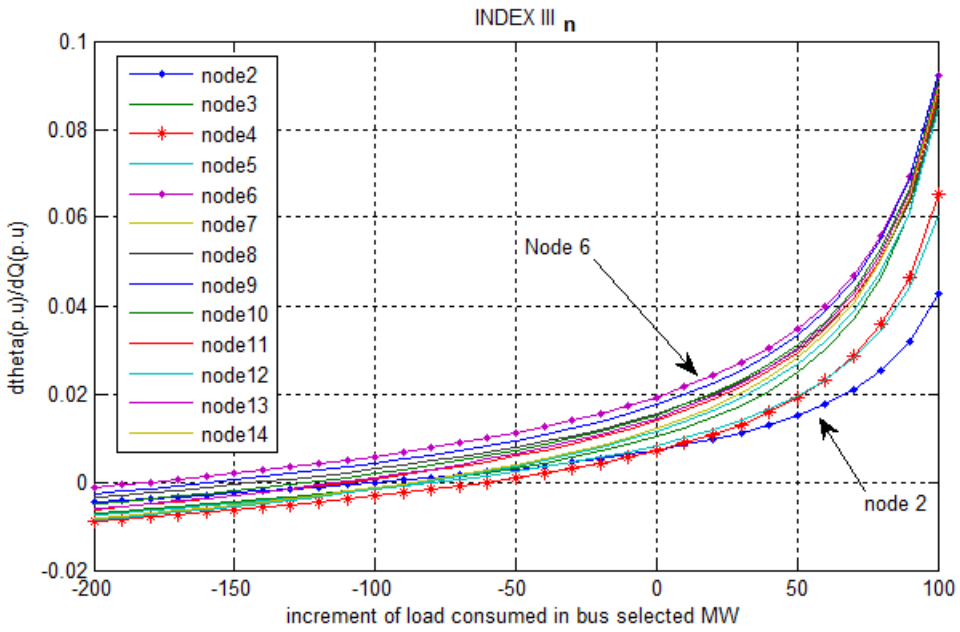

Figure 4.5: Index III obtained when changing the load at bus 3

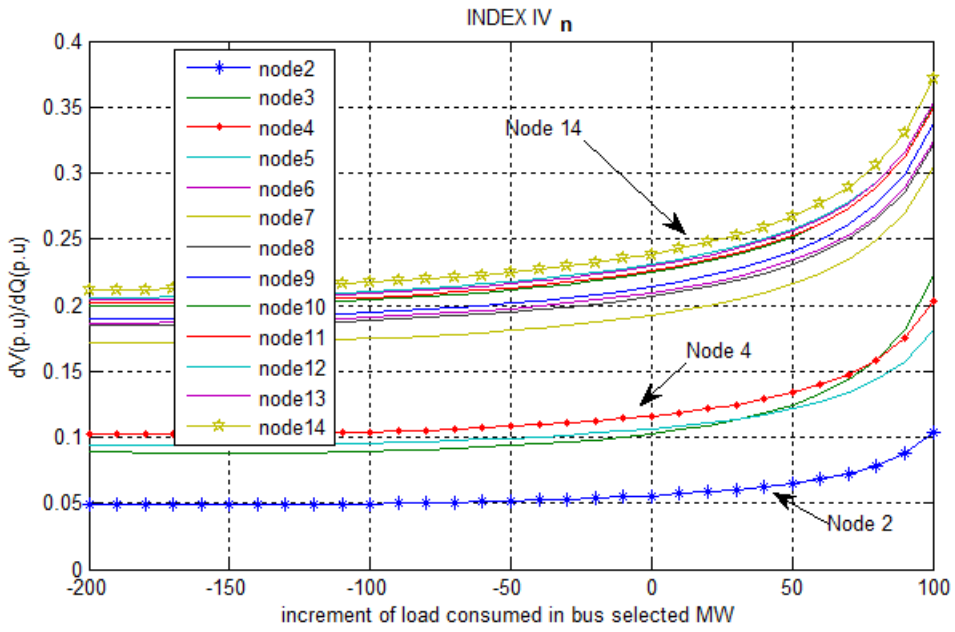

Figure 4.6: Index IV obtained when changing the load at bus 3

In general Bus 14 has the largest value for Indexes I, II and IV. The 14 Bus System is a loop transmission system, which is a characteristic of this kind of systems. In essence, the

behavior of Index III can be neglected since this one has an insignificant value compared to the other indexes.

In addition, one aspect that should be considered in this analysis consists in validating that the system operates within a stable range, that is why the eigenvalues of the Jacobean Matrix are monitored for this range of active power change at bus 3, the result is depicted in Figure (4.7). And as it is shown there, all eigenvalues appear on the right side of the complex plane, and so on the system operation is stable. This principle was explained in a previous chapters.

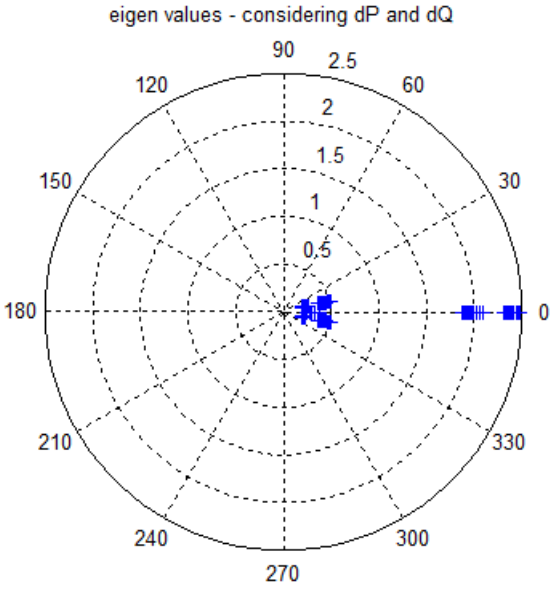

Figure 4.7: Eigen values obtained for the load change at bus 3

But let us consider a second calculation of the indexes, but in this case the load will be changed at some intermediate point in the system, such as bus 6. For the same amount of active power injection and demand forced at this bus, the following family of curves representing the indexes behavior is obtained.

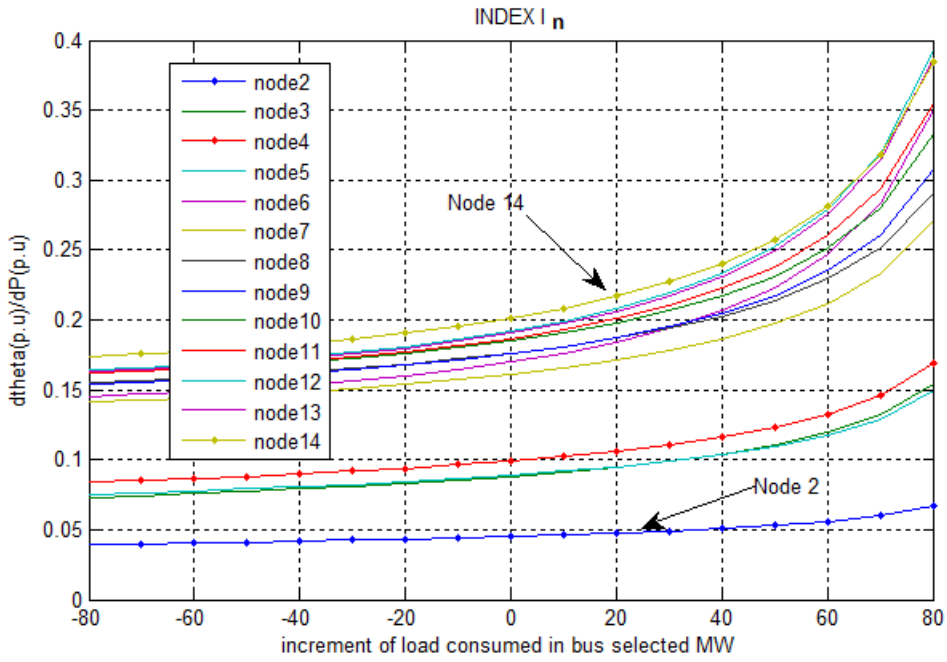

Figure 4.8: Index I obtained when changing the load at bus 6

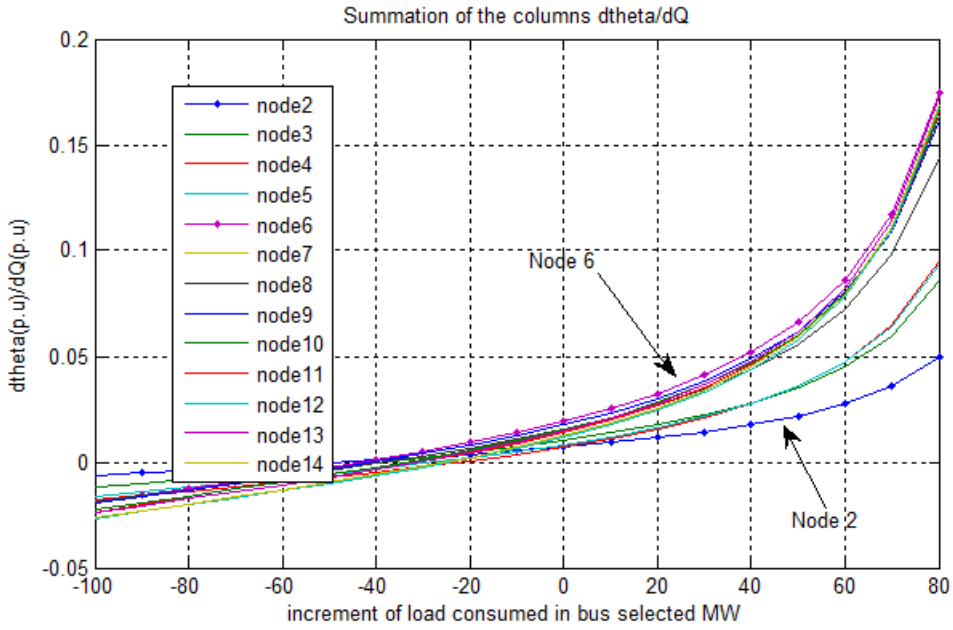

Figure 4.9: Index II obtained when changing the load at bus 6

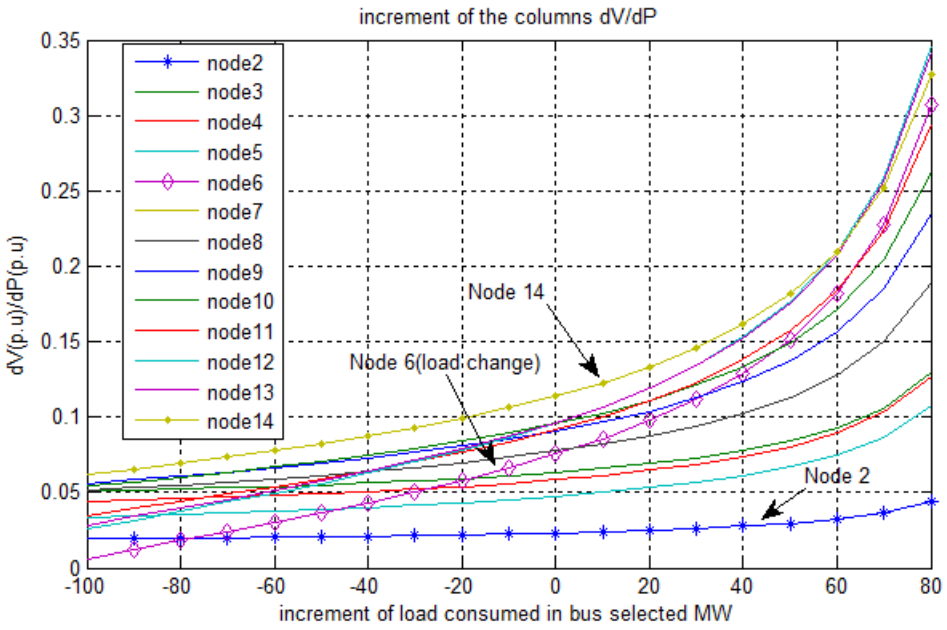

Figure 4.10: Index III obtained when changing the load at bus 6

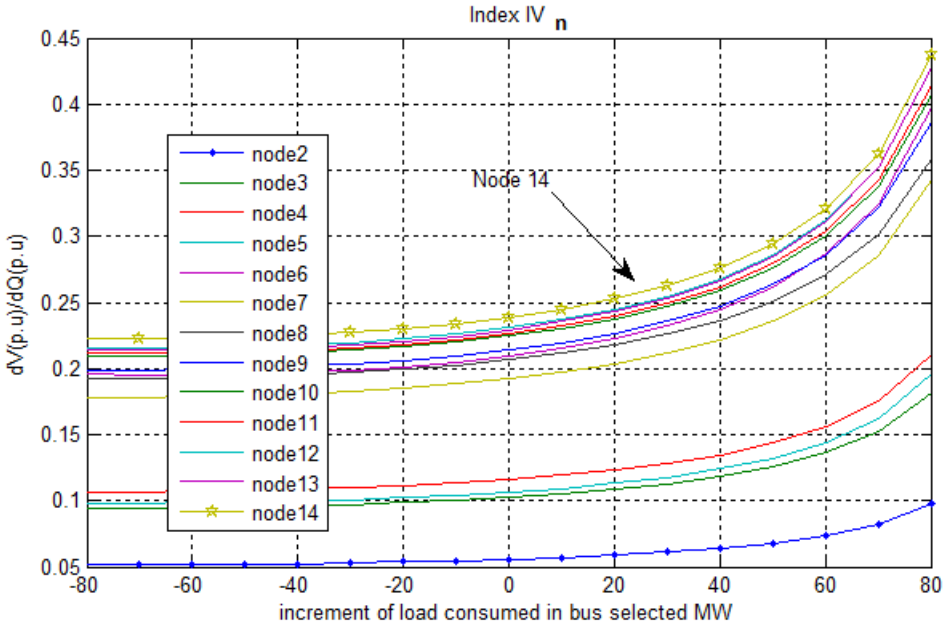

Figure 4.11: Index IV obtained when changing the load at bus 6

Again for the curves shown in figure (4.8)-(4.11), bus 14 has the largest value even though a small change is performed at bus 6 in this case. The main conclusion from this result, is that the indexes are not dependent on the place where the change in power is

done. Herein, the methodology shows the importance of calculating these four indexes as a result of the steady state calculation. Other aspect that has to be mentioned, and that also has a very important meaning, is that for most of the indexes, even though a considerable amount of load variation range is considered, the relative distance within different nodes appears during the entire range of load change; which means that in this particular case, bus 14 is the bus that according to the indexes will have the largest change in volts, when a power injection or increase in demand is forced at that point. Or in other words, if storage is placed at node 14, the change in volts magnitude for all the rest of the system will be greater, compared to all other possible storage location places.

Herein, a conclusion appears showing that a change in active power, has the largest effect on the rest of the voltage at other nodes, so if the system faces some low voltage scenario, the effect of discharging 1MW of power at bus 14 will have a higher impact on the system, and the voltage of the 14 buses will be backed up more efficiently.

5 Steady state methodology

The steady state methodology is depicted in figure (5.1). In this diagram, the main purpose is to show that the steady state planning methodology primarily calculates the indexes once the Newton-Raphson method converges to meet the requirements of the power flow. Therefore, a change in the loading condition is exhibited at some particular node in the system and the indexes are recalculated. It is possible to obtain a behavior that will establish a weighted measurement of the voltage and phase changes, depending on a change at an specific location.

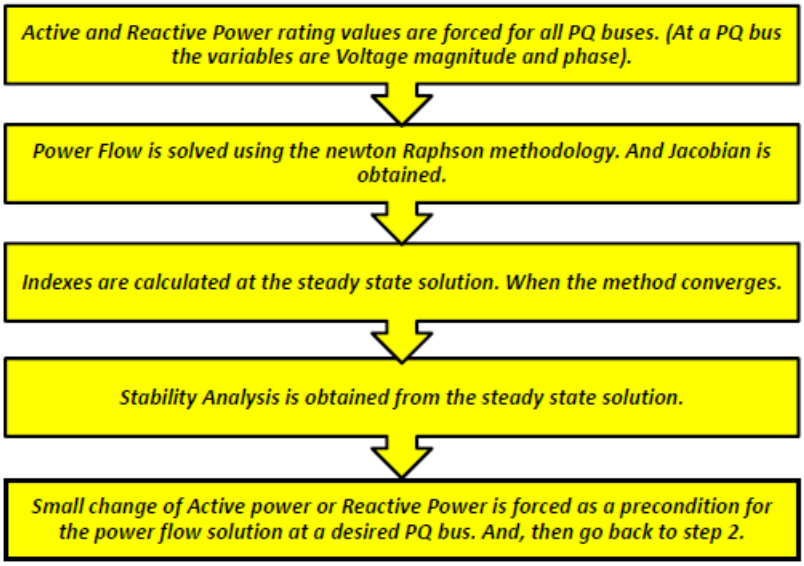

Figure 5.1: Diagram of the process used to calculate the indexes in a Microgrid

Different locations were tested, and it was found out that the relative behavior of the indexes for each one of the buses throughout the system, does not depend on the location of bus where the change in loading conditions is performed. Herein, the indexes depend only on the structure of the system, or in other words the line impedance architecture of the system. In the next chapter a systematic arrangement that was used in Matpower (Matlab tool) [6] will be shown and explained in detail.

5.1 Arrangement of the Power Flow code in Matpower for the sensitivity analysis

Matpower is a Power System planning tool box, detailed explanation about he software can be found in [6]. This subprogram was developed in the Matlab language, and allows the user to get a Power Flow solution using methods for non-linear equations solutions, such as: Newton-Raphson, Gauss-Seidel and Newton-Raphson decoupled, the last one mentioned is commonly used in Transmission systems due to the inductive nature of the line impedance.

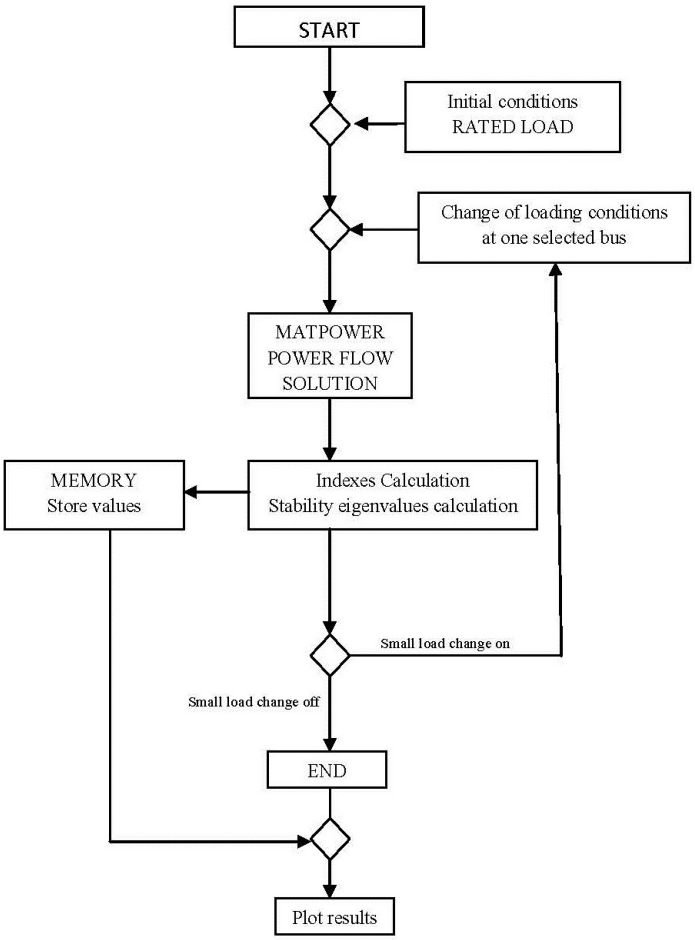

Figure 5.2: Diagram of the process utilized to program Matpower for the study

Figure (5.6) shows how Matpower changes its loading conditions, solves the power flow, and calculates the indexes for each loading condition. One of the main advantages

of this software is that the Matlab user can use Matpower as an input/output tool that can supply the values of Jacobean, obtained in the last iteration once the power flow has converged.

Four subprograms were used, based on the requirements of the study. In this thesis work the system that was used as the testing platform is the 34 Bus Distribution Test Feeder from the IEEE, which can be found at [4]. Some modifications were done on the system, this modifications will be discussed with more details in the next chapter.

Coming back to the four subprograms used, a summary of the programs used for the planning analysis methodology is shown in table 2 and 3. In these tables, inputs, outputs, analysis performed and hierarchy are exhibited. So that, a clear understanding of each one of the rolls in the code and calculations performed, allows the reader to have a clear understanding of the method proposed for indexing calculations.

MATLAB SUBPROGRAM	CALCULATIONS PERFORMED	HIERARCHY
storage_34_V2_updated.m	Main program - global variables	Master
stabilityI.m	Eigenvalues	slave
IndexesI.m	four Indexes calculation	slave
case34_mod5.m	Power Flow solution	slave

Table 2: Hierarchy and calculations performed by the subprograms used in the planning methodology for Battery storage placement

MATLAB SUBPROGRAM	INPUTS	OUTPUTS
storage_34_V2_updated.m	none	Indexes and eigenvalues plots
stabilityI.m	Jacobean Matrix	Eighteen-values
IndexesI.m	Jacobean Matrix	Indexes obtained for load condition
case34_mod5.m	Loading conditions	Jacobean matrix at the convergence point

Table 3: Input/Output of the Subprograms used in the planning methodology for Battery storage placement

One essential aspect to understand how the planning analysis tool was arranged, is to understand the data flow in a hierarchy based diagram. Figure (5.3) gives a detailed explanation of the connections between the subprograms utilized in this methodology.

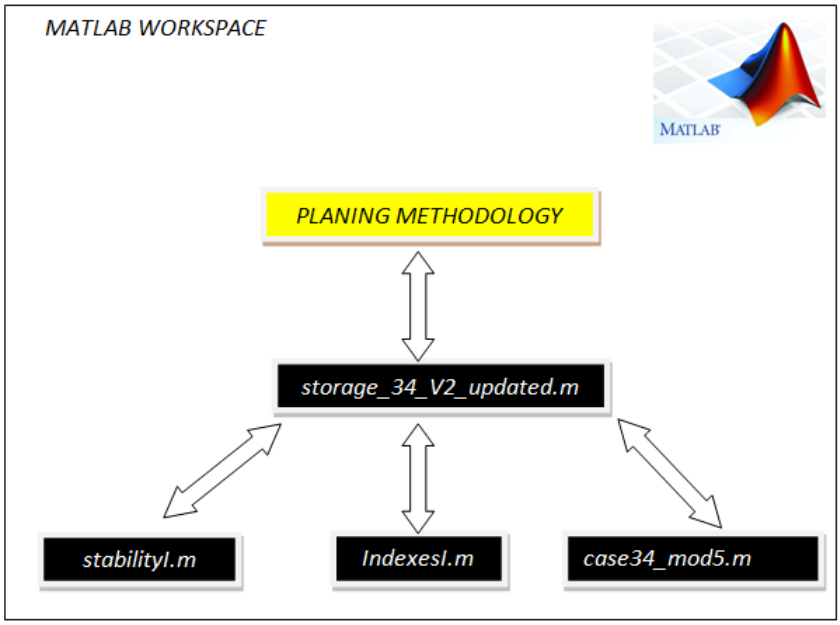

Figure 5.3: Hierarchy and data flow for the methodology proposed.

6 Location of the storage for a Distribution System case

Initially, it should be mentioned that for this study the system used was the 34 Node Test Feeder [4]. This system is a Distribution system and detailed explanation of the loading conditions and line configurations are available in the official site of the Power Energy Society (PES). `http://ewh.ieee.org/soc/pes/dsacom/testfeeders/`. The rated voltage value of the original system is 24kV, but the system was scaled down to 12kV guaranteeing the same voltage drop across the lines, and in this way make the system closer to a microgrid. The main considerations and changes are described in table 4

LINE IMPEDANCE PARAMETER	ORIGINAL 24KV SYSTEM	MODIFIED 12KV SYSTEM
Line capacitance	standard given value	Quadrupling the capacitance matrix
Line length (impedance matrix)	standard given value	halving the original length

Table 4: Main changes in the 34 Node IEEE System

6.1 Description of the system

The 34 Bus system has been used during this project as the testing platform. This system offers a wide variety of line models and load models. Mainly, constant impedance load models and constant PQ models. In order to prove the accuracy of the methodology two different approaches were done. This system also accounts for single lines that branch out from the main three phase feeder, and has the typical radial characteristic of distribution systems. Also, unbalance is a characteristic of this system.

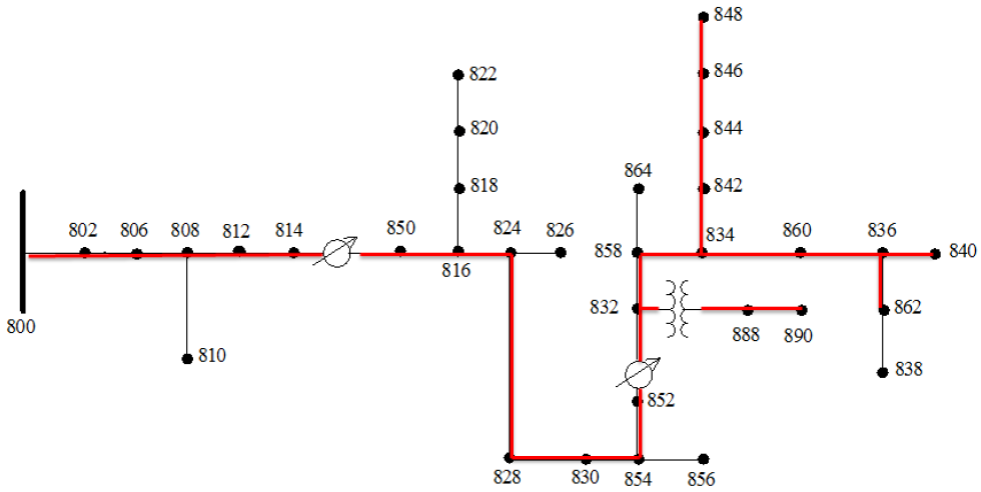

Figure 6.1: 34 IEEE Node Test Feeder. Distribution Standard PES. Main three phase feeder is highlighted.

As it is shown on (6.1), twenty six (26) nodes out of thirty four (34) nodes, are three phase buses. Also the system has two voltage regulators and a transformer which taps down the voltage from 12kV to 0.480 kV. Summing up, this test feeder was selected due to the amount of features that classify it as a real test case, that can be used to prove the methodology.

6.2 System setting up for the study

One of the main considerations is the steady state planning analysis which was computed for the 34 Bus System. The power flow solution available in Matpower only works for three phase balanced systems, but since the 34 Bus system is not a balanced system, some special considerations were included. The technique used to balance the system, was in essence keeping the same voltage drop conditions across the main three phase feeder. For that purpose, the active/reactive power flow going through the single or two phase lines was calculated, and replaced with a three phase balanced constant PQ loads, located at the same place . The system was modeled using Matpower.

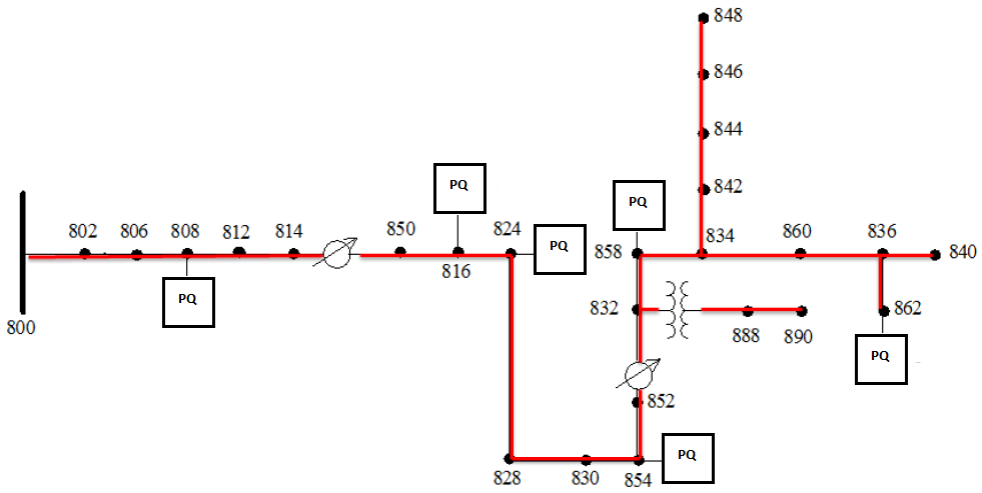

Figure 6.2: 34 IEEE Node Test Feeder. Distribution Standard PES. After pruning the single and two phase branches

One of the main characteristics that validates this averaging for the 34 Node IEEE System, is the one related to the fact that the average three phase voltage drop across the lines behaves almost the same. To show evidence of this consideration, average three phase voltages measured throughout the main three phase grid are shown in table 5 for the original system, and also for the transformed system.

THREE PHASE BUS	ORIGINAL (P.U)	AVERAGE (P.U)	ERROR $\lvert(\frac{original-Average}{original})\rvert$
800	1,05	1,05	0
802	1,048	1,048	0
806	1,047	1,047	0
808	1,025	1,025	0
812	0,999	0,9994	0,0004004
814	0,9787	0,9794	0,000715234
850	0,9786	0,9794	0,000817494
816	0,9784	0,9788	0,000408831
824	0,9696	0,9696	0
828	0,9687	0,9691	0,000412925
830	0,9517	0,9517	0
854	0,9512	0,9513	0,00010513
852	0,9211	0,9215	0,000434263
832	0,9211	0,9215	0,000434263
888	0,9035	0,9032	0,000319285
890	0,8830	0,8838	0,000980072
858	0,9188	0,9189	0,000108838
834	0,9116	0,9116	0
842	0,9158	0,9159	0,000109194
844	0,9155	0,9156	0,00010923
846	0,9156	0,9157	0,000109218
848	0,9157	0,9158	0,000109206
860	0,9154	0,9155	0,000109242
836	0,9152	0,9153	0,000109266
862	0,9153	0,9154	0,000109254
840	0,9151	0,9152	0,000109278
Summation of errors			0.006011
Summation of errors (%)			0,60106

Table 5: Three phase voltage average (p.u) comparison between the original and average system

As it was aforementioned, the idea of using Matpower changing the loading conditions at different locations allows us to prove one of the most important implications in the application of this methodology. This implication is:

"The results obtained for the indexes have the same relative behavior, regardless of where the change in load is performed, and depend mainly on the line infrastructure design".

6.3 Steady State Analysis for the storage location in the 34 Node IEEE System

As it was explained in Chapter 4, four indexes can be obtained for a power system, as long as, there is information available for the system architecture. From this point, the methodology can be extended and applied to any system. Now, the same procedure explained for the 14 Node IEEE Transmission System, is applied to the 34 Node IEEE Distribution System. But in this case, special emphasis will be done regarding the operation concerns in Microgrids.

Now it has to be mentioned that only "voltage stability" has been considered for the purpose of this thesis. So on, only the indexes related to voltage changes due to active and reactive power variations will be discussed and analyzed for the 34 Node IEEE System.

Before going into the analysis and interpretation of the indexes obtained for this case, it is very important to mention that the storage system is interfaced to the grid, through an inverter. This means that both active and reactive power control can be done. Or, in other words, active and reactive power can be injected or absorbed from the point where the storage is connected. Now, with this concept mentioned let us proceed to understand the meaning of the indexes obtained from the steady state planing methodology.

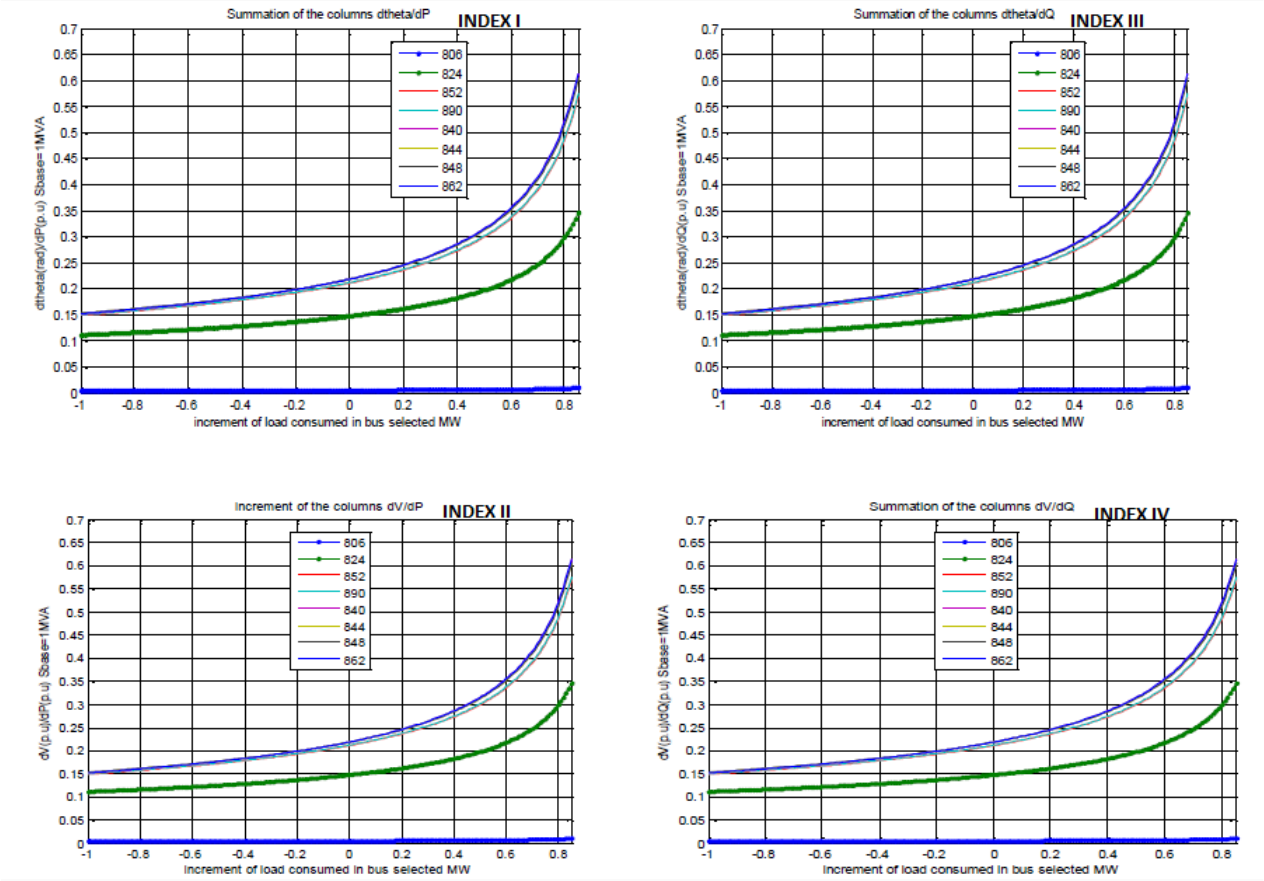

Figure 6.3: Index I, Index II, Index III and Index IV, obtained when changing the load at bus 830

First, the indexes are calculated following the steady state methodology proposed. Refer to Figure (6.3) to identify the locations that will be further discussed. The results obtained for indexes II and IV are shown in figures (6.4) and (6.5), for the possible candidates for storage placement, and also a location 824 has been selected, which is not a good location for the storage system. This location will be also discussed, as a way to show how beneficial the candidates are if storage system is placed there, instead of somewhere else in the system. Based on the curves obtained for a range of 500kW increase and decrease when changing the load at bus 830 in the system, Buses 848 and 862 have the largest value for the arbitrary range of load variation. This range was chosen for a technical reason that will be addressed in the next subsection, but in essence is the size of the inverter technology

used during the IAPS project.

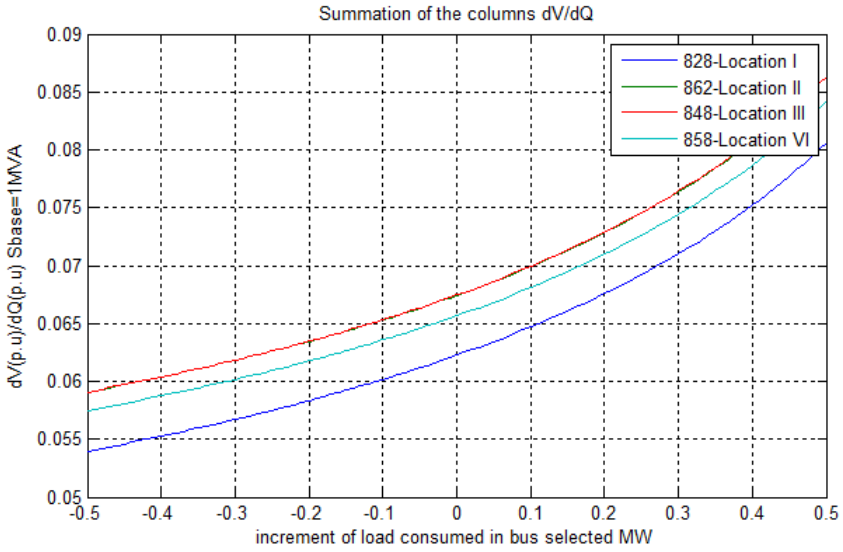

Figure 6.4: Index IV, $\frac{\partial |V|}{\partial Q}$ obtained when changing the load at bus 830

As shown in figure (6.4), Index IV values show that if storage is placed at bus 848 or 862, and 1MVAr is injected at one of these locations. Then, the largest average voltage increase per node is obtained, for all buses in the system. Or the other way around, for an increase in consumption of 1MVAr at one of this locations, the largest average voltage decrease per node is obtained for all buses in the system.

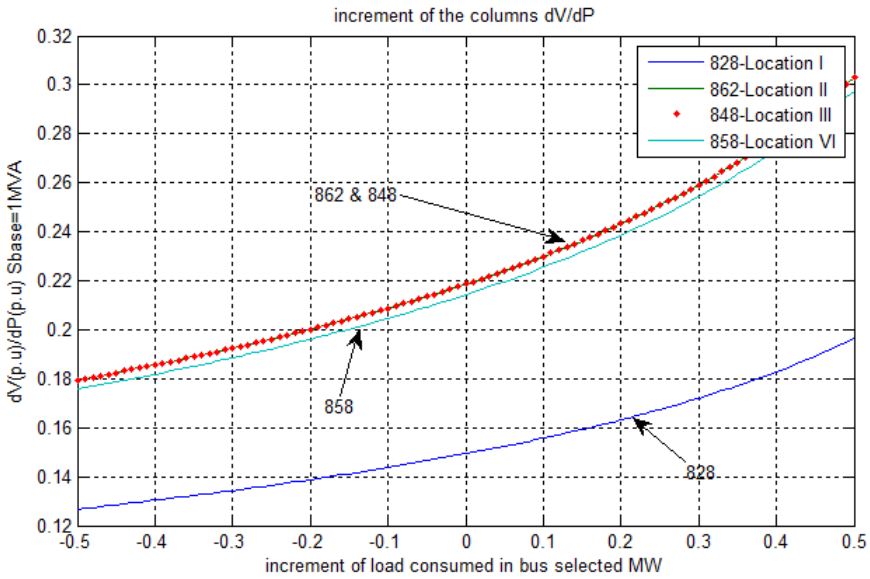

Figure 6.5: Index II, $\frac{\partial |V|}{\partial P}$ obtained when changing the load at bus 830

Same result is shown in figure (6.5), Index II values show that if storage is placed at bus 848 or 862, and 1MW is injected at one of these location. Then, the largest average voltage increase can be obtained, for all buses throughout the system.

One of the main consequences of finding possible candidates for the storage location using a steady state methodology, opens the possibility of deciding which are the possible locations for storage placement in larger systems. As it was shown and discussed before, immediately it can be seen that based on Index II and IV, location 828 has the lowest value for both indexes, which means storage will exhibit the smallest impact on the system, if installed at this location.

Now, that the two indexes have been explained, and analyzed for the purpose of placing the storage in the 34 Bus IEEE System. It is essential to show what is the impact on the voltage caused by that change in active power, due to a change in power at the possible storage locations obtained. Figures (6.6) and (6.7) show the voltages behavior for a range of load change from -500kW to 500kW at two different locations, nodes 824 and 862. Based on the previous analysis a change in load at bus 862 will exhibit a higher impact in voltage

change. For that purpose the slope has been calculated for three different intervals, within the same range of load change. Those intervals are $[-0.4 to -0.2MW]$, $[-0.2 to 0.2MW]$ and $[0.2 to 0.4MW]$. Again, just to clarify the idea once more, negative power in this case means generation or injection of active power at the node, positive power change means an increase in the power demand.

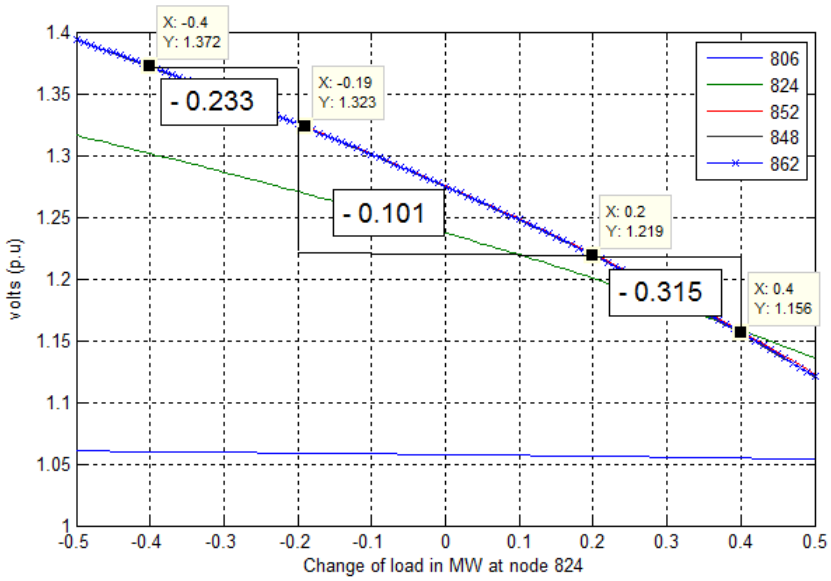

Figure 6.6: Voltages (p.u) obtained when changing the power at node 824. Calculation of the slope for node 852.

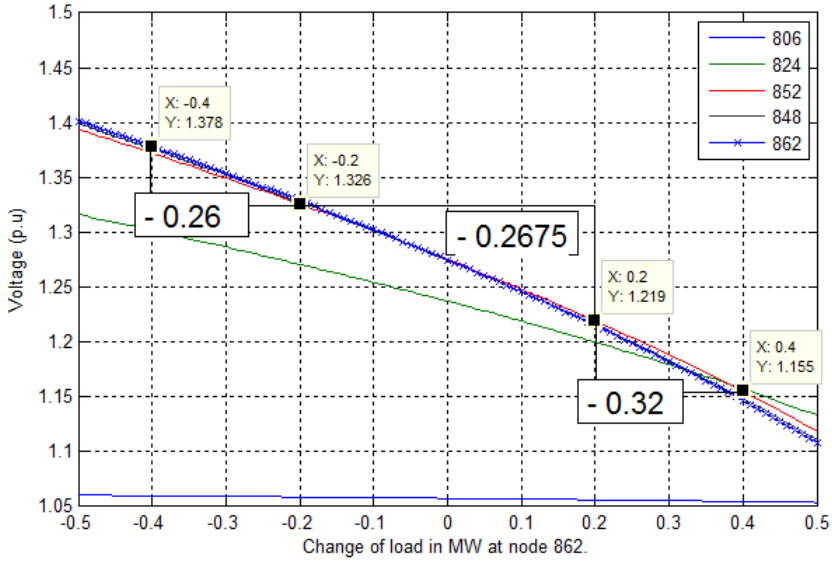

Figure 6.7: Voltages (p.u) obtained when changing the power at node 824. Calculation of the slope for node 852

To summarize the data available in figures (6.6) and (6.7). Table 6 shows the slope calculation for the voltage curves at the two different load change locations.

	SLOPE INTERVAL I	SLOPE INTERVAL II	SLOPE INTERVAL III
$\triangle P$ LOCATION.	$[-0.4 to -0.2 MW]$	$[-0.2 to 0.2 MW]$	$[0.2 to 0.4 MW]$
824	-0.233	-0.26	-0.315
826	-0.2675	-0.32	-0.32

Table 6: Slope values in $\frac{Voltage(p.u)}{P_{load}(MW)}$ calculated for three different almost linear intervals, from figures (6.6) and (6.7).

As it is shown on Table 6, the values for the slope in $\frac{Voltage(p.u)}{P_{load}(MW)}$ at interval I are smaller when the load is decreased, versus the values obtained for the interval of load increase. This result yields to the conclusion that the effect in changing volts per MW is greater when the load is increased, and the system is close to an unstable operating point. Also, this can be seen in the Index II and IV behavior shown in Figures (6.6) and (6.7), in which the value becomes greater when the load demand is increased.

7 Experimental Platform

In order to start this important discussion,which is in essence the experimental prove of the Method proposed. An aspect that has to be addressed regarding Microgrid operation, is related to four different modes of operation, such as:

- Islanded Mode
- Grid Connected Mode
- In transit from grid connected to isolated mode
- In transit from isolated mode to grid connected mode

Each one of these modes has unique power quality issues, that affect the stability of the system, and primarily the voltage stability.

Herein, in order to prove the accuracy of the methodology, the possible candidates to place the storage that were obtained using the steady state solution were tested using a transient analysis software called PSCAD. The model used for this purpose was obtained from the PSCAD group and also scaled to 12kV [1], using the same methodology previously mentioned. This model offers a wide variety of detailed models, such as voltage regulators, unbalanced line models, different load models and also the possibility of building controls to include models for wind generation, solar PV generation, battery storage, etc [10]. All of them equipped with an average inverter model that operates in a voltage source current control mode [1].

The main advantage of using the 34 Node System in PSCAD, is that a real time simulation result can be obtained to assess the effect of storage in different locations.

Since the steady state methodology shows that Buses 862 and bus 848 are the best locations for storage, the following four locations are selected to simulate the same storage locations in PSCAD and validate the methodology. The four locations selected, and the values of the indexes related to the voltage change are shown in Table 7.

NO.	STORAGE LOCATION	INDEX II - $\frac{\partial \lvert V \rvert}{\partial P}$(P.U)	INDEX IV - $\frac{\partial \lvert V \rvert}{\partial Q}$(P.U)
I	848	0.22	0.0675
II	862	0.22	0.0675
III	858	0.215	0.0663
IV	828	0.15	0.062

Table 7: Indexes II and IV for the storage Locations selected in (p.u). Bases of 12kV - 1MW -1MVAr

The testing in PSCAD was performed for three different Microgrid operating modes, and for each one of the modes, four locations for battery storage were tested:

7.1 Battery Discharging at 300kW in a low voltage scenario

For this simulation, the 34 Bus System is run at the peak load (*1.8MW*) in the isolated mode (*Diesel 2MVA)*. A 500kW ZBB Battery equipped with an inverter average model (Avoiding switching) interface to the grid, is connected at the four different locations. The voltages are monitored throughout the three phase feeder, before and after the battery is discharged. Both voltages results are captured once the steady state has been accomplished by the Diesel Generator *(Governor response and Excitation response is at the steady state).* Figure (7.1) shows the architecture of the system and the four different locations tested.

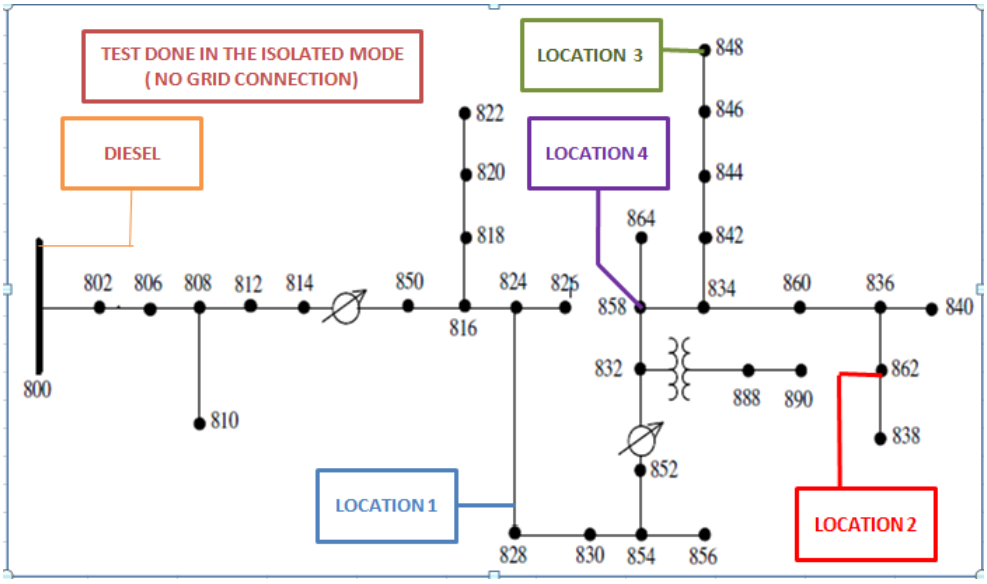

Figure 7.1: 34 IEEE Node Test Feeder. Distribution Standard PES.

After the testing was done and the values of voltage were captured at both steady states. The data shown in figure (7.2) was obtained. This figure shows the *three phase average volt increase change in (p.u)*, after the battery is discharged at 300kW *(60% of the rated power of the 500kW ZBB Battery)*. From the three dimensional figure it can be observed that location I (node 828) has the lowest increase in voltage (p.u) throughout the main feeder. And, Location II (node 862), Location III (node 862) and Location (IV) have a similar increase in voltage after the battery has been discharged. But how to decide whether location II, III or IV is more effective per node. To solve this issue an idea similar to the one used for the steady state indexes was used. In this case, for the twenty six *(26)* three phase buses an arithmetical average was computed, and the results are shown in Figure (7.3).

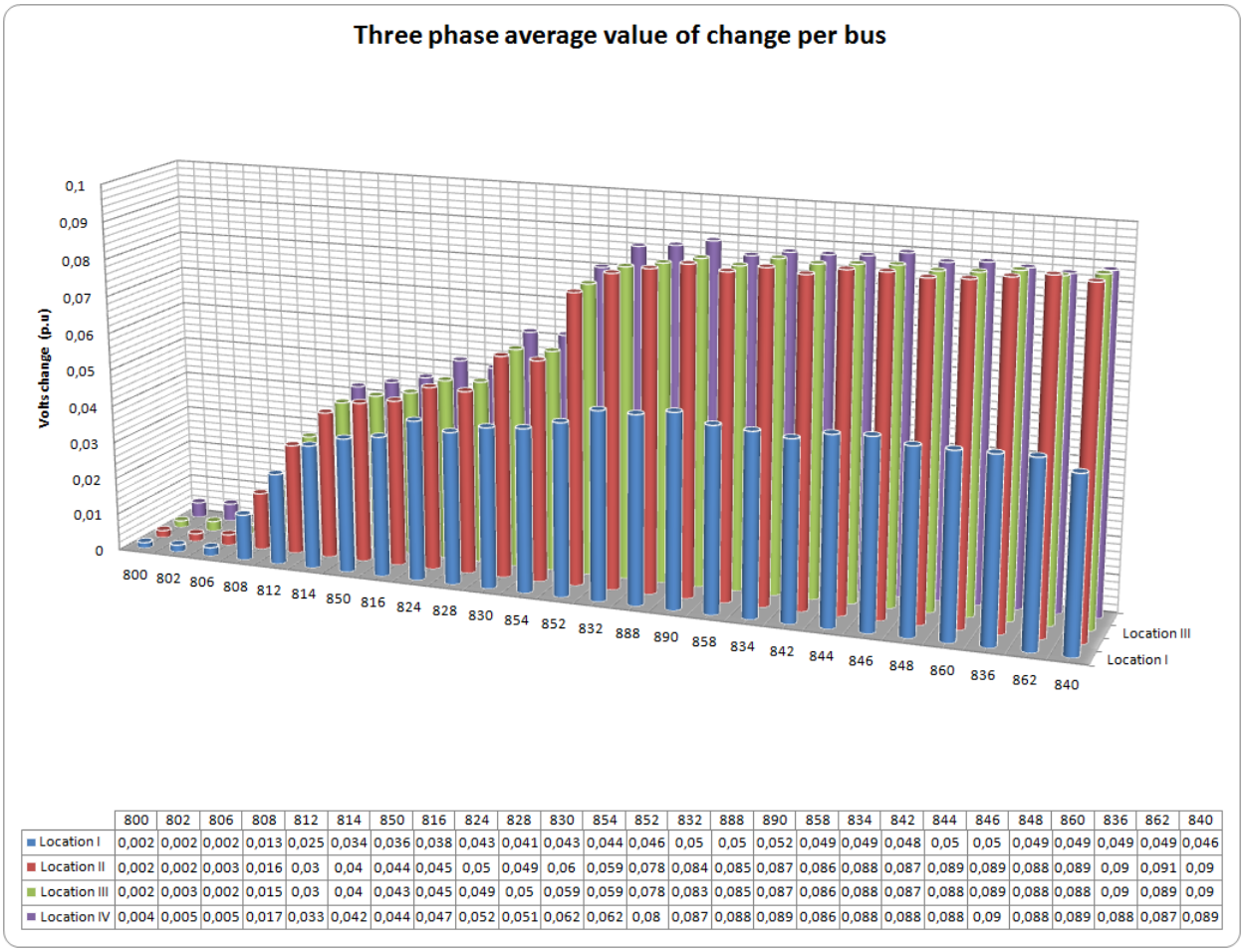

	800	802	806	808	812	814	850	816	824	828	830	854	852	832	888	890	858	834	842	844	846	848	860	836	862	840
Location I	0,002	0,002	0,002	0,013	0,025	0,034	0,036	0,038	0,043	0,041	0,043	0,044	0,046	0,05	0,05	0,052	0,049	0,049	0,048	0,05	0,05	0,049	0,049	0,049	0,049	0,046
Location II	0,002	0,002	0,003	0,016	0,03	0,04	0,044	0,045	0,05	0,049	0,06	0,059	0,078	0,084	0,085	0,087	0,086	0,088	0,087	0,089	0,089	0,088	0,089	0,09	0,091	0,09
Location III	0,002	0,003	0,002	0,015	0,03	0,04	0,043	0,045	0,049	0,05	0,059	0,059	0,078	0,083	0,085	0,087	0,086	0,088	0,087	0,088	0,089	0,088	0,088	0,09	0,089	0,09
Location IV	0,004	0,005	0,005	0,017	0,033	0,042	0,044	0,047	0,052	0,051	0,062	0,062	0,08	0,087	0,088	0,089	0,086	0,088	0,088	0,088	0,09	0,088	0,089	0,088	0,087	0,089

Figure 7.2: Change in Volts for four different storage locations discharging the battery at 300kW.

As it is shown on figure (7.3), the average increase in volts, for the three phase nodes in the system, has a slightly larger value for location II, compared to location III and IV. However, location I has the lowest value in backing up the voltage, as expected from the steady state calculation.

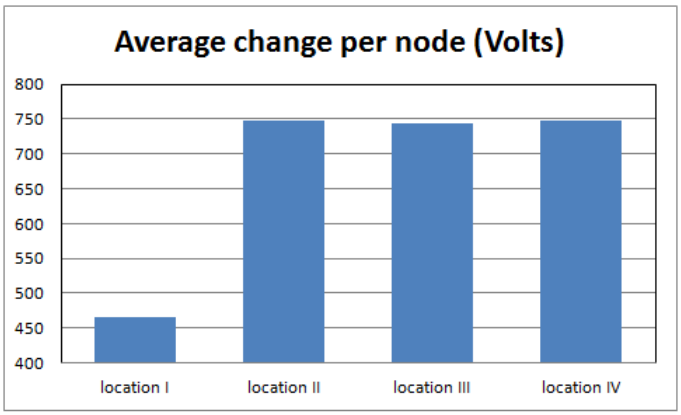

Figure 7.3: Average change per node in Volts for four different storage locations when injecting 300kW

Moreover, the differences obtained for locations II, III and IV are not large enough to desist from placing the storage at one of these locations. So, another simulation was executed in order to include variables such as Renewable Energy Location, but this aspect will be recapitulated later on the chapter.

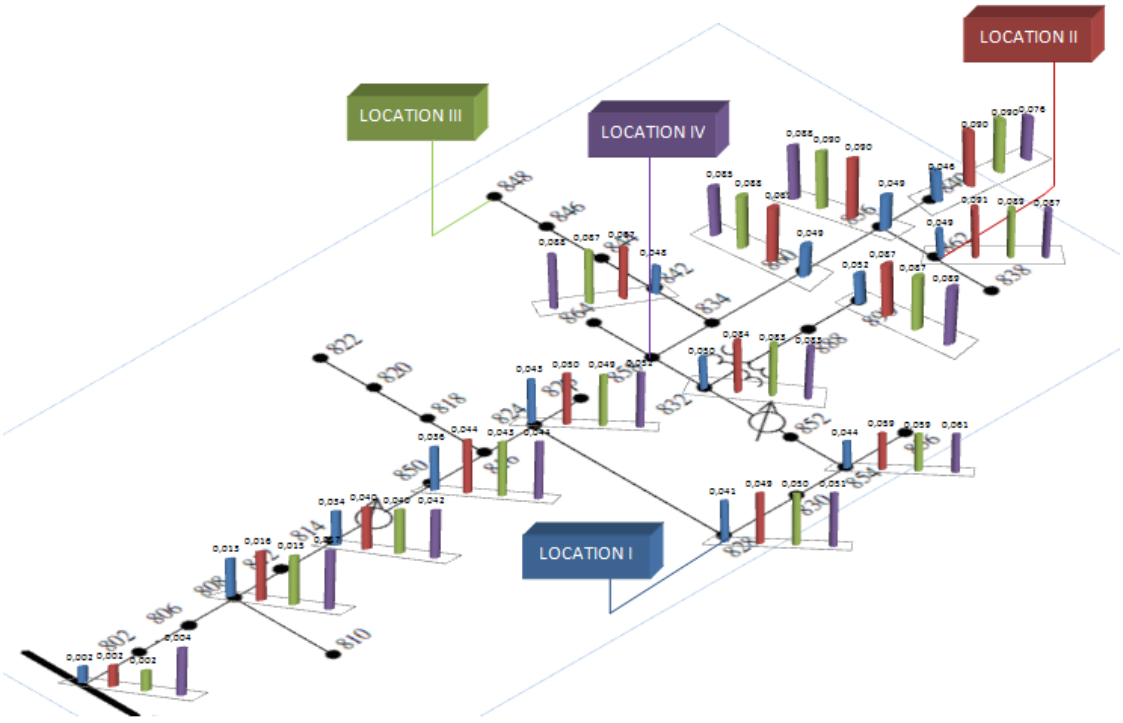

Figure 7.4: Histogram per node of the increase in Voltage (p.u), after the battery is discharged at 300kW in the isolated mode.

In addition, the diesel response was captured right after the battery discharges 300kW, for the four different storage locations. The transient experienced by the 2 MW Diesel Generator connected at bus 800, is shown for the four storage locations on Figure (7.5) . The battery command to discharge is activated arbitrarily at 5 seconds, and the action of the governor and exciter of the machine can be seen as well. It can be concluded from the Diesel Generator behavior, that when storage is installed at Location I, the active power requirement from the generator is less compared to the other locations. Important to enhance this conclusion mentioning, that the active power shown is the total summation of the active power from each phase of the generator, which are unbalanced since the system is unbalanced.

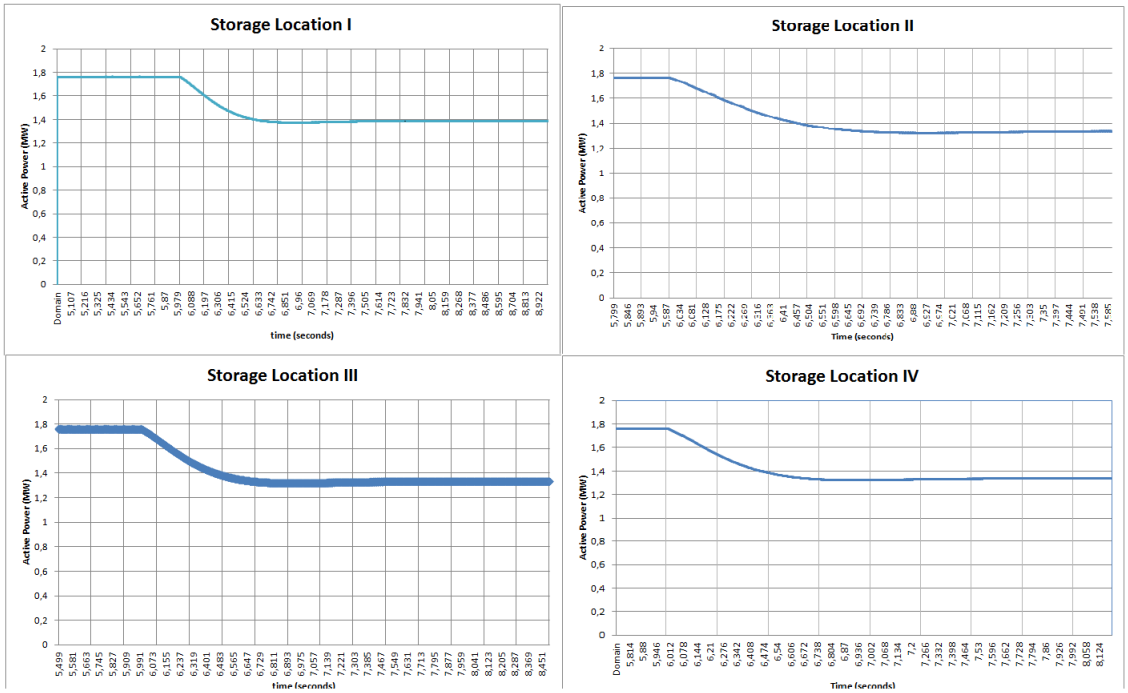

Figure 7.5: Active Power generated by the Diesel Generator in (MW). Transient experienced by the generator once the ZBB Battery is discharged at 300kW

Now, that the $\triangle P$ value is known to be 300kW injection. It is possible to compute the experimental result obtained from PSCAD, dividing the average increase in voltage that was calculated before, and then dividing by the power injected. The results from computing this value are shown in Figure (7.6). From Figure (7.6) one result that sets a precedent in

the accuracy of the methodology, is that the value obtained for $\frac{dV}{dP}$ is in the range of 0.2, which is very close to the change in voltage calculated from the steady state methodology. Somehow, it can be said at this point that the steady state methodology can predict which range of voltage (p.u) can be changed for an injection of 1MW from the storage system, when installed at some particular location.

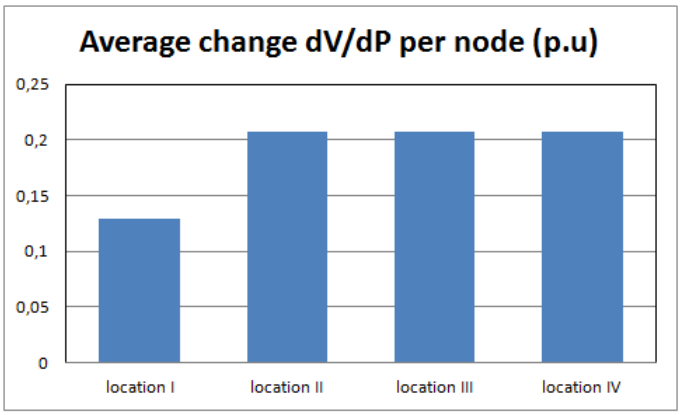

Figure 7.6: Active Power generated by the Diesel Generator in (MW). Transient experienced by the generator once the ZBB Battery is discharged at 300kW

7.2 Battery Charging at 400kW in a high voltage scenario

In order to enhance the result obtained from the steady state methodology, a second scenario was tested. In this scenario, arbitrarily three different locations for renewable energy sources (*Active Power injection*) were selected. The locations are in essence at the end of the branches of the system, and also are three phase buses of the system. Herein, in order to emulate the effect of injecting renewable energy power into the system, the technique used was to shed some load in the vicinity of the renewable energy. As a result the system faces a high voltage scenario, and so on the purpose of the storage system in this case is to charge, in order to force a decrease in the voltage level throughout the system nodes.

Four different locations for storage were tested and a scheme of the system, renewable energy locations, and storage locations tested are shown in Figure (7.7). Here, the nature of renewable energy in not transcendental, since the analysis targets only the steady state

response of the system after the ZBB Battery is charged at 400kW.

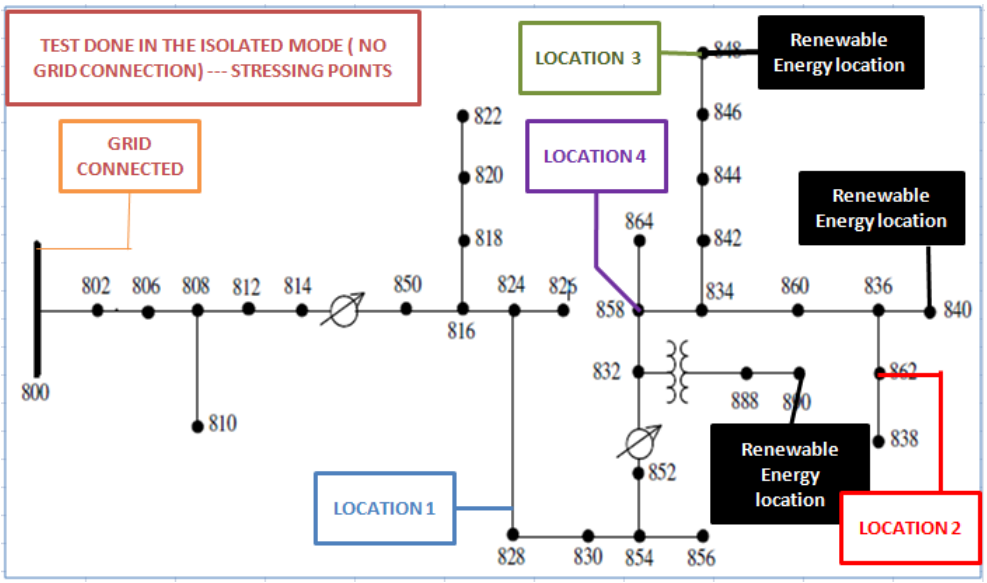

Figure 7.7: 34 Node IEEE System in the Grid connected mode with Renewable energy locations arbitrarily placed

The same calculation was computed for this scenario, but in this case the change in voltage is a decrease after the battery charges. It is important to mention that not necessarily all phases behave in the same way, but the average three phase voltage obtained reflects a decrease after the battery discharge. The decrease in voltage, measured in (p.u), is shown in Figure (7.8).

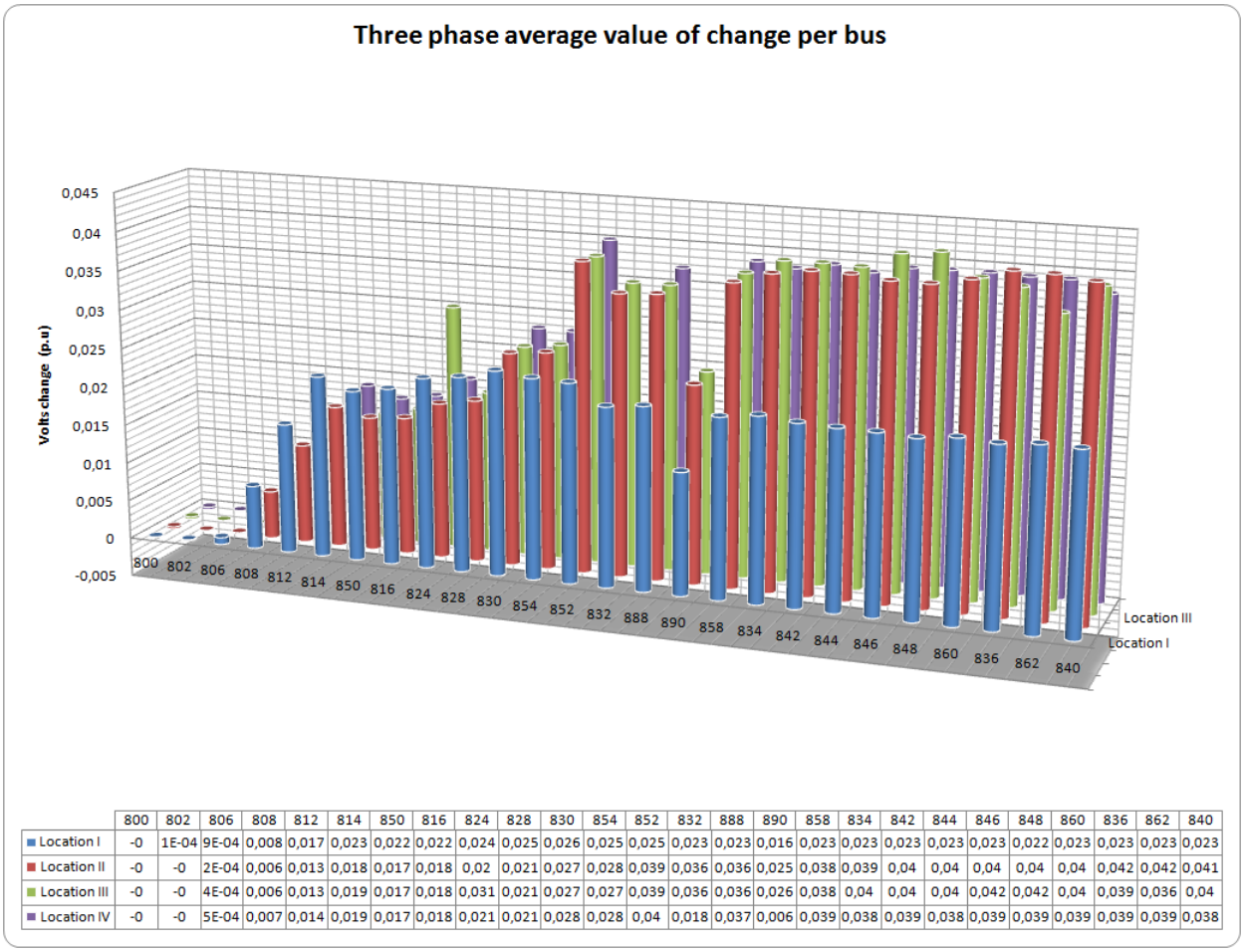

	800	802	806	808	812	814	850	816	824	828	830	854	852	832	888	890	858	834	842	844	846	848	860	836	862	840
Location I	-0	1E-04	9E-04	0,008	0,017	0,023	0,022	0,022	0,024	0,025	0,026	0,025	0,025	0,023	0,023	0,016	0,023	0,023	0,023	0,023	0,023	0,022	0,023	0,023	0,023	0,023
Location II	-0	-0	2E-04	0,006	0,013	0,018	0,017	0,018	0,02	0,021	0,027	0,028	0,039	0,036	0,036	0,025	0,038	0,039	0,04	0,04	0,04	0,04	0,04	0,042	0,042	0,041
Location III	-0	-0	4E-04	0,006	0,013	0,019	0,017	0,018	0,031	0,021	0,027	0,027	0,039	0,036	0,036	0,026	0,038	0,04	0,04	0,04	0,042	0,042	0,04	0,039	0,036	0,04
Location IV	-0	-0	5E-04	0,007	0,014	0,019	0,017	0,018	0,021	0,021	0,028	0,028	0,04	0,018	0,037	0,006	0,039	0,038	0,039	0,038	0,039	0,039	0,039	0,039	0,039	0,038

Figure 7.8: Average change in voltage (p.u) after charging the battery at 400kW, measured throughout the three phase buses in the system

Again, for this case Location I exhibits the shortest decrease in voltage throughout the three phase nodes of the system. And, as expected from the steady state methodology proposed, the effect of charging a battery placed at location II, III and IV is much higher. In order to quantify the effect per node, an arithmetical average is computed, the result is shown in Figure (7.9).

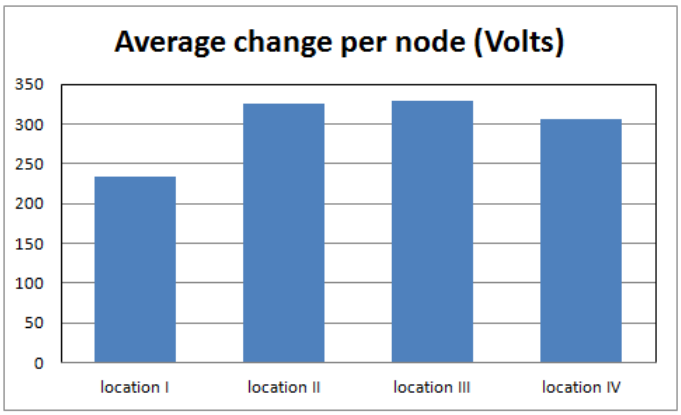

Figure 7.9: Average change in voltage (p.u) per node after charging the battery at 400kW

Based on the results from Figure (7.9), it can be again concluded that Locations II, III and IV exhibit a much higher voltage decrease. But, from the experimental results Location IV seems to have a better impact than others, even though the values are very close for Locations II, III, and IV.

An extra calculation that has to be computed, as a way to prove the accuracy of the steady state methodology is the one related to the $\frac{dV}{dP}$ obtained, taking advantage that the power charged by the battery is a known variable. The results obtained for the second scenario tested are shown in Figure (7.10). Based on the results obtained from charging the battery, it can be concluded that location II, and III have the largest $\frac{dV}{dP}$ calculated. So, once more it is proved that the methodology holds when charging the battery.

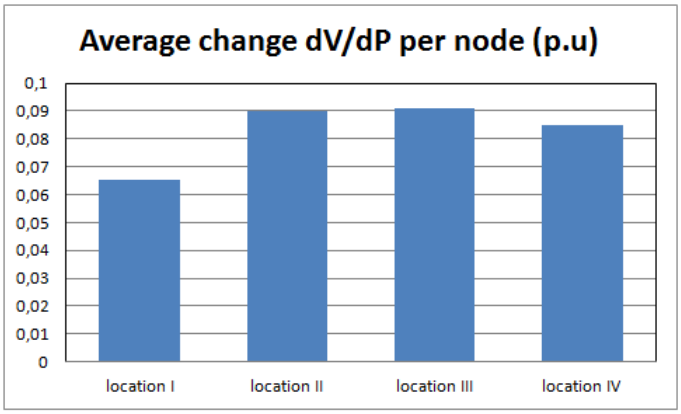

Figure 7.10: Average change in voltage (p.u) per node after charging the battery at 400kW

7.3 Real time scenario

Up to this point, the testing results calculated have been only focus on the steady state response of the system. But in order to prove the effectiveness of the storage at different locations, a more realistic simulation was done. In this case, wind profiles and insulation profiles for the city of Milwaukee were obtained for the Summer 2002. Also a variable load model was included in the system.

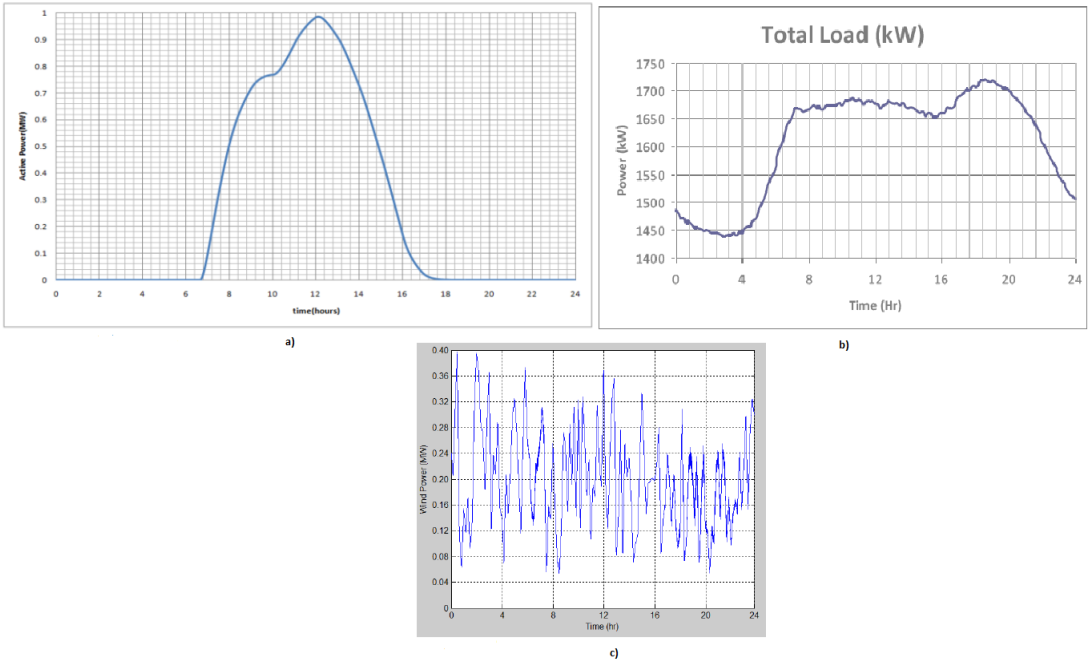

Figure 7.11: Renewable energy profiles used in the 24 hours simulation. a) Power profile for a 1MW PV generator. b) Total Load of the system. c) Power profile for a 0.4 MW Wind Farm.

All renewable energy models are scalable, and also are interfaced with the grid through an average inverter model. The inverter can regulate active/reactive power injected to the system. The 24 hours real time simulation includes: (2) two 1MW Wind Generators, (1) 0.25 MW PV Generator, (1) 500kW ZBB Battery and a variable load model as the one shown in Figure (7.11). The locations for each device are depicted in Figure (7.12), and also (17) monitoring locations are symbolized with a blue box. The importance of defining this locations, is that based on the voltage measurements the effectiveness of placing the

storage can be assessed.

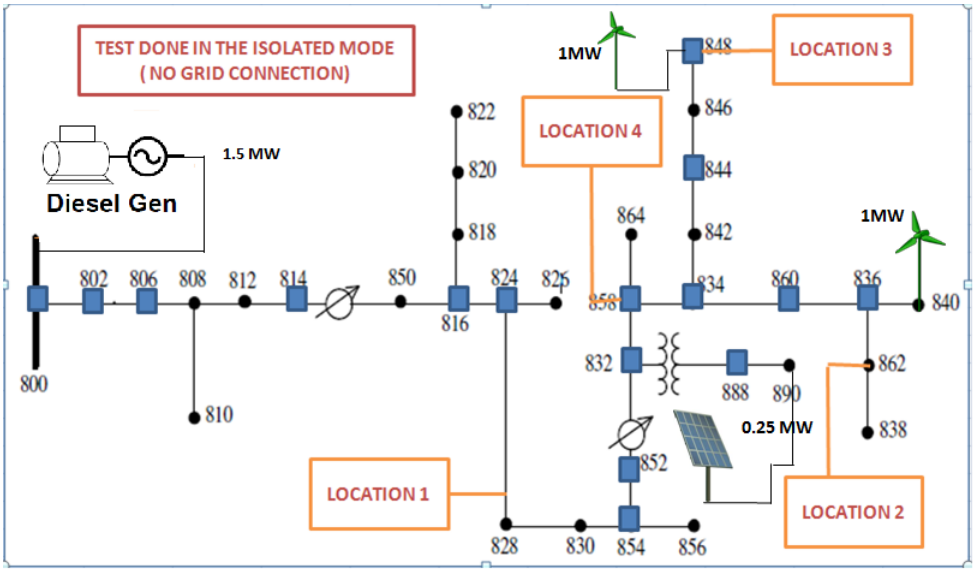

Figure 7.12: Configuration of the Microgrid used as testing platform for the 24 hour simulation.

The following list of indexes were calculated running the system for 24 hours, and changing the location of the ZBB Battery:

- Number of voltage high voltage violations for 24 hours. *A high voltage violation is defined as the increase of voltage above 1.05 p.u, staying above this value before the system controls react to set it down* .
- Number of voltage low voltage violations for 24 hours. *A low voltage violation is defined as the decrease of voltage below 0.92 p.u, staying below this value before the system controls react to push it up.*
- Time duration for high voltage and low voltage during 24 hours. *Time in minutes the voltage stayed above 1.05 p.u and below 0.92 p.u*
- Index of storage charging effectiveness (SCE). This index is mathematically defined

as shown in equation (7.1).

$$SCE = \frac{total\ high\ voltage\ duration\ (min)}{total\ energy\ charged\ (MWh)} \tag{7.1}$$

- Index of storage discharging effectiveness (SDE). This index is mathematically defined as shown in equation (7.1).

$$SDE = \frac{total\ low\ voltage\ duration\ (min)}{total\ energy\ discharged\ (MWh)} \tag{7.2}$$

As it was mentioned before, the idea of assessing this (4) indexes for each storage location, is that a clear idea of the effect of storage placement can be obtained. An aspect that has to be mentioned, is that each generator in the system is equipped with controls that will heal the voltage and frequency of the system. Those controls are discussed more in detailed in [10]. But, to get an idea the controls are: *Active Power Curtailment and Reactive Power Support.*

Now, let us proceed to analyze each one of the results. First, the number of high voltage violations for 24 hours, is shown on Figure (7.13). Here, only storage locations I, II and IV are shown. Location III was omitted due to the fact that a wind farm is connected at the same node, and some technical aspects as synchronization of the PLL to measure phase becomes a drawback. So on, the voltage throughout the system is completely unstable.

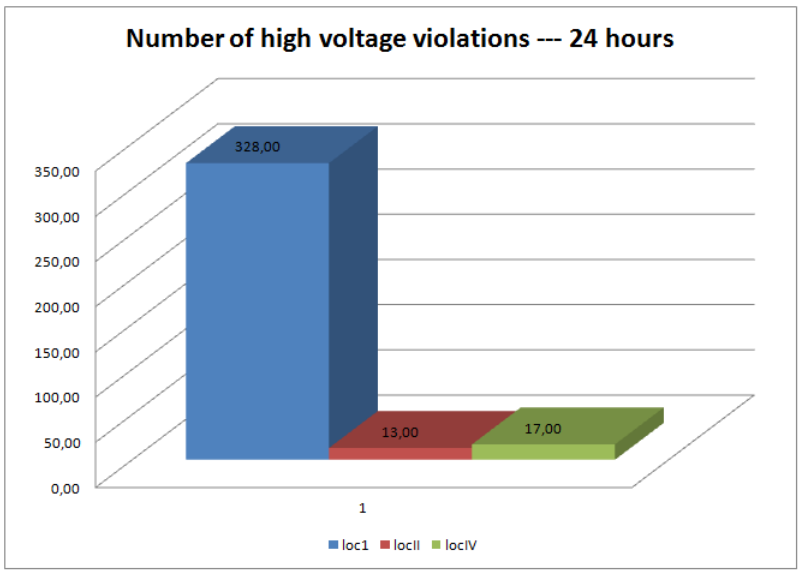

Figure 7.13: Number of high voltage violations recorded at the (17) monitoring locations, for a 24 hour simulation and three different storage locations.

Based on the result shown on Figure (7.13), location I shows the largest number of high voltage violations recorded at the monitoring devices. Location II and IV have very close results, but Location II exhibits 13 high voltage violations, versus 17 violations for Location IV . A conclusion from this result, is that the effect of installing the battery storage system at location II has a higher impact in maintaining the voltage below 1.05 p.u. This result enhances once more the steady state methodology, in which Location II and IV were suggested candidates by the Indexes. And the candidate locations exhibit a great performance during a 24 hours real time scenario.

Also, the total number of low voltages recorded at the monitoring places are shown in Figure (7.14) for storage locations I, II and IV. As shown in this figure, once more Location II and IV exhibit a much better performance throughout the 24 hours simulation. Though, it has to be commented that location IV exhibits a better performance, in the sense of having less low voltage scenarios.

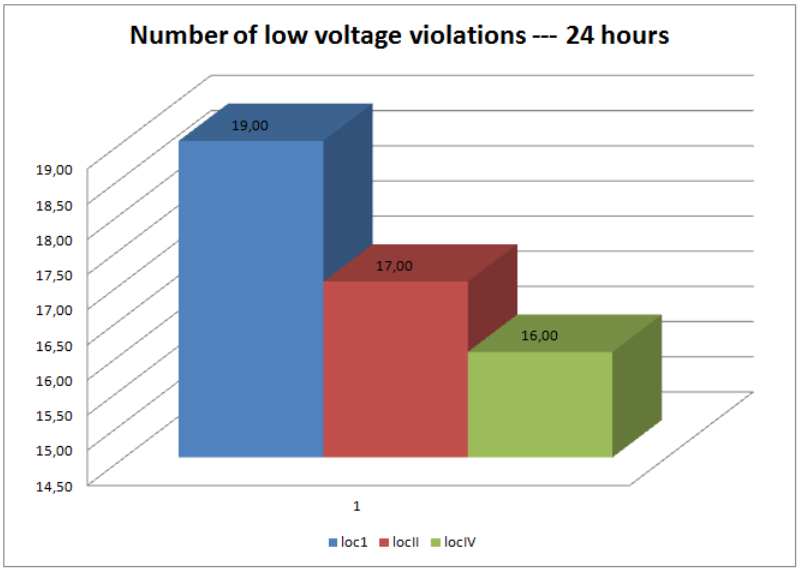

Figure 7.14: Number of low voltage violations recorded at the (17) monitoring locations, for a 24 hour simulation and three different storage locations.

However, one important aspect that has to be addressed is the time the voltage was above 1.05 p.u, and below 0.92 p.u. Here, the recordings obtained for the (17) monitoring places are added up, and shown in figure (7.15). From the results shown here, it can be concluded again that the effect of the storage if placed at location II or IV, has a larger impact in decreasing the total time, that voltages monitored were above 1.05 in at least 86 % in comparison with Location I (*This location was classified previously as a bad candidate for the storage placement, based on the indexes from the steady state methodology*).

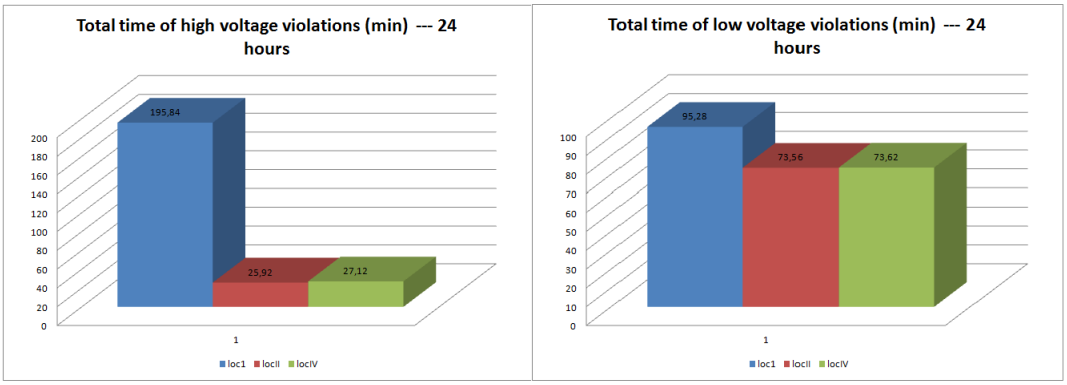

Figure 7.15: Time summation for all (17) monitoring devices in minutes

Moreover, Figure (7.15) also shows the total time monitored at the (17) locations, that the voltage was below 0.92 p.u. The result shows once more, that for a 24 hours simulation, Location II, and IV have a much better performance than Location I. And, compared to Location I, Locations II and IV have a 20 % improvement.

As defined in equations (7.1) and (7.2), two indexes were calculated for the three different storage locations. The results obtained for the SCE and SDE in $\frac{1}{MW}$ are shown in Figure (7.16). These indexes can be understood as the effect of either charging or discharging the battery, in an effort to maintain the voltage level within a stable range (1.05 to 0.92 p.u) for a 24 hours simulation. As it is shown in Figure (7.6), location I has the largest SCE and SDE, which means for 1MW of active power charged or discharged, the effect in keeping the voltage within a stable range is less, than if the same 1MW is charged or discharged at locations II or IV. In other words, the higher the SCE or SDE is the less effective the storage discharge or charge is to the system.

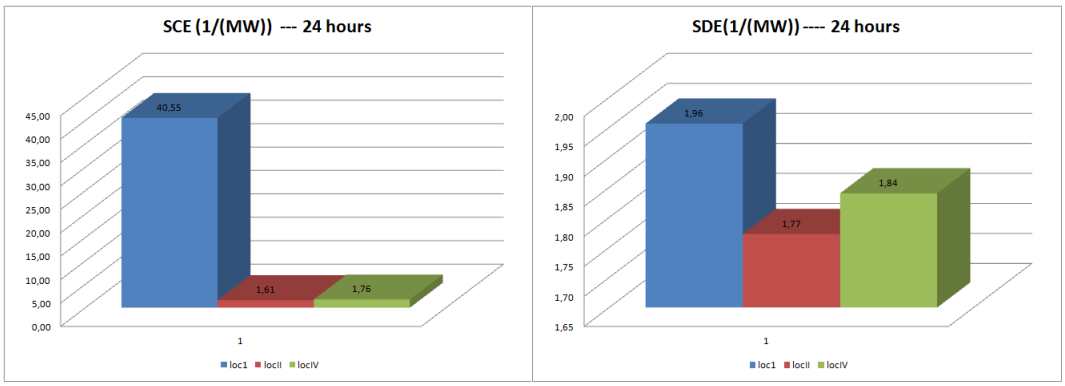

Figure 7.16: SCE and SCD in $\frac{1}{MW}$ for locations I, II and IV.

8 Conclusions

- Storage location II and IV, which were candidates obtained using the steady state methodology. Show an excellent performance when tested using PSCAD (Transient Analysis Program)
- Indexes I, II, III and IV obtained from the steady state methodology were validated in the real time 24 hours simulation.
- The result shows a milestone in deciding where to place the storage in Microgrids, with renewable energy penetration.
- A methodology which can predict the effect of storage at different locations was developed, based on an extension of Power Flow Analysis.
- The results shown by the testing platform show a complete correlation with the results obtained using the Novel Planning methodology.

References

[1] Q. Fu, A. Solanki, L. F. Montoya, Student Members, IEEE A. Nasiri, Senior Member, IEEE, V. Bhavaraju, Senior Member, IEEE, and D. Yu, Senior Member, Generation Capacity Design for a Microgrid for Measurable Power Quality Indexes, IEEE Conference Paper, IEEE. ISGT Conference 2012.

[2] Carson W. Taylor, Power System Voltage Stability, McGraw-Hill Inc, Appendix B, 1994.

[3] A. R. Bergen, Power Systems Analysis, Prentice-Hall, Englewood Cliffs, NJ, 1986.

[4] IEEE PES Distribution System Analysis, Subcommittee's Distribution Test Feeder Working Group-IEEE Standards, Distribution test feeders, `http://ewh.ieee.org/soc/pes/dsacom/testfeeders/`

[5] 1547 IEEE Standard for Interconnecting Distributed Resources with Electric Power Systems. 2003.`http://grouper.ieee.org/groups/scc21/1547/1547_index.html`

[6] Matpower User's Manual. A Matlab Power System Simulation Package. Version 3.2. `http://www.pserc.cornell.edu/matpower/`

[7] Voltage Stability Analysis comparing Generator Sensitivity based Method with V-Q Curve Method for Optimal Placement of STATCOM, Neena Ramesh, B.V Sanker,Vedam Subrahmanyam, International Journal of Computer Applications (0975 – 8887), Volume 38– No.12, January 2012 `http://research.ijcaonline.org/volume38/number12/pxc3876822.pdf`

[8] Power System Sensitivity Analysis for Probabilistic Small Signal Stability Assessment in a Deregulated Environment Zhao Yang Dong, Chee Khiang Pang, Pei Zhang, International Journal of Control, Automation, and Systems, vol. 3, no. 2 (special

edition), pp.355-362, June2005 http://ijcas.com/admin/paper/files/IJCAS_v3_n2_pp.355-362.pdf

[9] IEEE Transmission System. 14 Node IEEE Standard. http://www.ee.washington.edu/research/pstca/pf14/pg_tca14bus.htm

[10] Managing Intermittent Renewables in a Microgrid A. Solanki, L. F. Montoya, Q. Fu, Student Members, IEEE, A. Nasiri, Senior Member, IEEE, V. Bhavaraju, Senior Member, IEEE, and D. Yu, Senior Member, IEEE. ISGT Washington DC, 2012.